ARTICLE INFO:
Received : April 13, 2018
Revised : August 01, 2018
Accepted : March 26, 2019
CT&F - Ciencia, Tecnologia y Futuro Vol 9, Num 2 December 2019. pages 15 - 35
DOI : https://doi.org/10.29047/01225383.178

ecopetrol
ctyf@ecopetrol.com.co

OPTIMAL SHAPE PARAMETER FOR MESHLESS SOLUTION OF THE 2D HELMHOLTZ EQUATION

PARÁMETRO ÓPTIMO DE FORMA PARA LA SOLUCIÓN DE LA ECUACIÓN DE HELMHOLTZ 2D EN MODELO SIN MALLA

Mauricio-A, Londoño[a]; Hebert, Montegranario[a].*

ABSTRACT

The solution of the Helmholtz equation is a fundamental step in frequency domain seismic imaging. This paper deals with a numerical study of solutions for 2D Helmholtz equation using a Gaussian radial basis function-generated finite difference scheme (RBFFD). We analyze the behavior of the local truncation error in approximating partial derivatives of the 2D Helmholtz equation solutions when the shape parameter of RBF varies. For discretization, we performed, by means of a classical numerical dispersion analysis with plane waves, a minimization of the error function to obtain local and adaptive near optimal shape parameters according to the local wavelength of the required solution. In particular, the method is applied to obtain a simple and accurate solver by using stencils which seven nodes on hexagonal regular grids, wich mitigate pollution-effects. We validated numerically that the stability and isotropy are enhanced with respect to Cartesian grids. Our method is tested with standard case studies and velocity models, showing similar or better accuracy than finite difference and finite element methods. This is an efficient way for interacting with inverse and imaging problems such as Full Wave Inversion

RESUMEN

La solución de la ecuación de Helmholtz es una parte fundamental en la modelación sísmica en el dominio de la frecuencia. Este artículo realiza un análisis numérico de las soluciones de la ecuación de Helmholtz 2D utilizando un esquema de diferencias finitas (RBFFD), generado por funciones gaussianas de Base radial. Se analiza el comportamiento del error de truncamiento local al aproximar las derivadas parciales de las soluciones de la ecuación de Helmholtz 2D cuando varía el parámetro de forma de la RBF. Para la discretización, hemos realizado, mediante un análisis de dispersión clásico con ondas planas , una optimización de la función de error para obtener valores locales y adaptativos del parámetro de forma de acuerdo con la longitud de onda local de la solución requerida. En particular, el método se aplica para obtener un programa sencillo y óptimo usando plantillas de siete nodos sobre mallas regulares hexagonales, que mitigan el efecto polución. Se comprueba numéricamente que la estabilidad e isotropía son mejoradas con respecto a las mallas cartesianas. Nuestro método es probado con casos de estudio y modelos de velocidad estándar, mostrando exactitud similar o mejor que los métodos de diferencias o elemento finitos. Esta es una manera eficiente de interactuar con problemas inverso y de imagen tales como la inversión de onda completa

KEYWORDS / PALABRAS CLAVE

RBF-FD | Helmholtz equation | Shape parameter | pollution effect.
RBFFD | Ecuación de Helmholtz | Parámetro de forma | Efecto polución

AFFILIATION

[a]Instituto de Matematicas, Universidad de Antioquia
Calle 67 53-108, Medellin, Colombia
*email: alejandro.londono@udea.edu.co

1 INTRODUCTION

The Helmholtz equation is an elliptic partial differential equation that represents time-independent solutions of the wave equation. This equation models a wide variety of physical phenomena. These include among others, acoustic wave scattering, time harmonic acoustic, electromagnetic elds, water wave propagation, membrane vibration and radar scattering. All these applications make getting accurate numerical solution for the Helmholtz equation the object of a large number of investigations and methods such as finite differences spectral elements, finite elements method and boundary elements.

Intended for of seismic modeling and inversion, this paper deals with the problem of acoustic and constant density wave propagation on a rectangular domain Ω by solving the Helmholtz equation.

$$-\Delta u(\mathbf{x}) - \omega^2 c(\mathbf{x})^{-2} u(\mathbf{x}) = f(\mathbf{x}) \qquad (1)$$

where ω is angular frequency, c(x) > 0 is a smooth function that represents the propagation speed of the wave and f(x) is a compactly supported distribution in ω that represents the source distribution. We consider boundary conditions (Dirichlet, Neumann and absorbing boundary conditions [5]) on the border $\delta\Omega$ and perfectly matched layers(PML) [1],[16] on an artificial extended domain a $\Omega_\delta \supset \Omega$.

When solving (1) at high frequencies by standard numerical methods the wavelength of the numerical solution is different than the real one $\lambda(x) = 2\pi/k(x)$, where $k(x) = \omega c(x)^{-1}$ is the so-called wavenumber. This discrepancy of wavelengths is known as pollution effect[2],[17]. To obtain a better solution, it is necessary to oversample the solution by increasing the number of points per wavelength N_g, which has as drawback more computational cost, time and memory. For these and other facts the design of fast and stable solvers for Helmholtz equation has become a significant computational challenge.

Seismic information of good quality about the earth's subsurface structures is the rationale for geophysical applications. The oil and gas industry uses computational intensive algorithms to provide an image of the subsurface. Information is obtained by sending elastic energy into the subsurface and recording the signal required for a seismic wave to be reflected back to the surface from the Earth interfaces that may have different physical properties. In the petroleum industry, accurate seismic information for such a structure can help in determining potential oil and gas reservoirs in subsurface layers. The seismic wave is usually generated by shots of known frequencies, placed on the earth's surface, and the returning wave is recorded by instruments also placed along the earth's surface.

Helmholtz equation solutions are essential in frequency domain seismic imaging methods such us full waveform inversion (FWI), which requires to solve this equation several times [34]. The traditional Finite Element Method (FEM) or standard Finite Differences (FD) produce sparse matrices but for a few degrees of freedom, there may be a strong pollution effect for large values of the wavenumber. [3],[4],[38] obtain solvers that mitigate the pollution effect in the high frequency regime. Recently, [13] developed a solver by using numerical micro-local analysis and ray-based finite elements method to achieve accurate local finite element space. Furthermore, global radial basis functions are more accurate but produce full matrices that become unstable.

Recently, [25] proposed a RBF-FD solver for frequency domain wave propagation and suggested that the approximated solution does not disperse at relatively high frequencies. In [8] There is an up to date view of the theory and applications of Radial Basis Functions and RBF-FD methods in the numerical solution of partial differential equations with examples in Geosciences and seismic problems.

This paper develops and applies a RBF-FD method on hexagonal grids that solves the Helmholtz equation for a wide range of values of the wavenumber k, focusing in obtaining accurate local approximations of the partial derivative operators by using a few degrees of freedom. Direct solvers may be applied to the banded matrices obtained; in particular we use UMFPACK.

2. THEORICAL FRAMEWORK

RBF INTERPOLATION

interpolation with Radial Basis Functions the objective is to reconstruct a d-variate function u defined on a bounded domain $\Omega \subset \mathbb{R}^d$ from the values $u(x_k)$ of u on a finite set of N scattered points $X = \{x_1, x_2, \ldots, x_N\} \subset \Omega \subset \mathbb{R}^d$. A radial basis function with shape parameter ε is defined as $\Phi_\varepsilon : \mathbb{R}^d \times \mathbb{R}^d \to \mathbb{R}$ [6],[31], [34] such that $\Phi_\varepsilon(x,y) = \phi(\varepsilon||x-y||)$, where $\phi : [0,\infty) \to \mathbb{R}$ is an univariate function. A sufficiently smooth function $u : \mathbb{R}^d \to \mathbb{R}$ can be approximated by the interpolant.

$$\mathcal{P}_{X,\varepsilon} u(\mathbf{x}) = \sum_{j\ 1}^{N} \alpha_j \Phi_\varepsilon(\mathbf{x}, \mathbf{x}_j). \qquad (2)$$

By forcing the condition $P_{X,\varepsilon} u(x_k) = u(x_k)$ for $k = 1,\ldots,N$, the weights α_j can be determined by solving the linear system.

$$u(\mathbf{x}_k) = \sum_{j=1}^{N} \alpha_j \Phi_\varepsilon(\mathbf{x}_k, \mathbf{x}_j), \ \text{with } k = 1, \ldots, N, \qquad (3)$$

provided that the interpolation matrix $\Phi_{X,\varepsilon} = \Phi_\varepsilon(x_k, x_k))_{1 \le k,j \le N}$ is non-singular and hence the interpolant $P_{X,\varepsilon} u$ with

$$\begin{pmatrix} \alpha_1 \\ \vdots \\ \alpha_N \end{pmatrix} = (\Phi_{X,\varepsilon})^{-1} u|_X. \qquad (4)$$

In particular, applying the Gaussian function $\phi(r) = e^{-r^2}$, the interpolation matrix $\Phi_{X,\varepsilon}$ is positive definite. Some important results about the convenience and properties of interpolation with this function can be found in [6].

The order of the approximation $u(x) \approx P_{X,\varepsilon} u(x)$ can be measured by the fill distance of X in Ω defined by

$$h_{X,\Omega} = \sup_{\mathbf{x}\in\Omega} \min_{1\le j\le N} \|\mathbf{x}-\mathbf{x}_j\| \tag{5}$$

and the stability [34] by the separation distance of X defined by

$$q_X = \frac{1}{2} \min_{1\le j\ne k\le N} \|\mathbf{x}_j-\mathbf{x}_k\|. \tag{6}$$

It is worth noting that RBF interpolation is meshless because it can be applied to scattered data with no dependence on point distribution. This property and the values of the shape parameter $\boldsymbol{\varepsilon}$ are commonly used to choose a geometry that may improve some performance or relevant aspects of the problem.

GLOBAL COLLOCATION METHOD WITH RBF

In recent years there has been increasing interest for obtaining approximated solutions of partial differential equations by the collocation method via RBF interpolation, either by unsymmetrical collocation or symmetric collocation [29]. Details for the latter can be consulted in [35]. Next, the unsymmetrical method will be described [19]. Under the RBF interpolation framework, we want to approximate the solution of boundary value problems in the formula

$$\begin{cases} \mathcal{L}u(\mathbf{x}) = f(\mathbf{x}) & \mathbf{x}\in\Omega \\ \mathcal{B}u(\mathbf{x}) = g(\mathbf{x}) & \mathbf{x}\in\partial\Omega, \end{cases} \tag{7}$$

where $\mathcal{L}$ and $\mathcal{B}$ are linear partial differential operators with regular coefficients have a regularity that is good enough. It is assumed that (7) it is a well-posed problem. Let $X=\{x_i\}_{i=1}^N \subset \Omega\cup\partial\Omega$ be a set of points conveniently separated as $\{x_i\}_{i=1}^m \subset \Omega$ and $\{x_i\}_{i=1}^N \subset \partial\Omega$. If it is supposing that the unique solution of (7) can be approximated by the interpolant $P_{X,\varepsilon}$ in (2), the problem may be forced by the equations

$$\begin{cases} \sum_{j=1}^N \alpha_j \mathcal{L}\Phi_\varepsilon(\mathbf{x},\mathbf{x}_j)|_{\mathbf{x}=x_k} = f(\mathbf{x}_k) & \mathbf{x}_k\in\Omega \\ \sum_{j=1}^N \alpha_j \mathcal{B}\Phi_\varepsilon(\mathbf{x},\mathbf{x}_j)|_{\mathbf{x}=x_k} = g(\mathbf{x}_k) & \mathbf{x}_k\in\partial\Omega, \end{cases} \tag{8}$$

arising from the linear system

$$\begin{pmatrix} \mathcal{L}\Phi_{\varepsilon,X\cap\Omega} \\ \mathcal{B}\Phi_{\varepsilon,X\cap\partial\Omega} \end{pmatrix} \begin{pmatrix} \alpha_1 \\ \vdots \\ \alpha_N \end{pmatrix} = \begin{pmatrix} f|_{X\cap\Omega} \\ g|_{X\cap\partial\Omega} \end{pmatrix} \tag{9}$$

and by (4), obtaining the following linear system whose unknowns are the u values at the points of X

$$\begin{pmatrix} \mathcal{L}\Phi_{\varepsilon,X\cap\Omega} \\ \mathcal{B}\Phi_{\varepsilon,X\cap\partial\Omega} \end{pmatrix} (\Phi_{\varepsilon,X})^{-1} u|_X = \begin{pmatrix} f|_{X\cap\Omega} \\ g|_{X\cap\partial\Omega} \end{pmatrix} \tag{10}$$

To get the approximated solution $\tilde{u}$ from (10), it is necessary that the collocation matrix $(\mathcal{L}\Phi_{\varepsilon,X\cap\Omega}\ \mathcal{B}\Phi_{\varepsilon,X\cap\partial\Omega})^t$ be non-singular, which in general is not true. An elaborated counterexample using multiquadrics and Gaussians was presented in [15]. However, under certain conditions, unsymetrical collocation method is feasible from a generalized approach using separated trial and test spaces [23],[24].

DISCRETIZATION BY RBF-FD

For problems requiring to compute solutions on large domains good resolution, the resultant matrix obtained by the collocation method is dense, huge and ill-conditioned, implying a prohibited computational cost. A variant of RBF collocation method enabling to deal with large domains is the local version [33],[36]. A local interpolation is possible to obtain a sparse matrix that represents the linear partial differential operator. This approach is often called Radial Basis Function-generated Finite Differences method (RBF-FD). The RBF-FD method is the following.

Let $X=\{x_i\}_{i=1}^N \subset \Omega\cup\partial\Omega$ be a set of interpolation points. For any $x_i \in X$ an influence domain $S_i \subset X$ is created which is formed by the n_i nearest neighbor interpolation points. That is, consider an n_i-stencil $S_i=\{x_j^i\}_{j=1}^{n_i} \subset X$, where $x_1^i \equiv x_i$ and $\Omega_i = \text{ConvexHull}(S_i)$. This is how the subsets $\{S_i\}_{i=1}^N$ of points contained in X. $u(x)$ are formed, which be approximated by RBF interpolation for $x\in S_i$ as

$$u(\mathbf{x}) \approx \tilde{u}(\mathbf{x}) = \mathcal{P}_{S_i,\varepsilon_i} u(\mathbf{x}) = \sum_{j=1}^{n_i} \alpha_j^i \Phi_{\varepsilon_i}(\mathbf{x},\mathbf{x}_j^i). \tag{11}$$

with $x\in\Omega_i$. On the shape parameter ε_i is on depending on the location x_i. This allows to manipulate the shape of the RBF according to known data. Collocating the n_i points of the stencil S_i, results in a small linear system given by

$$\Phi_{S_i,\varepsilon_i}\boldsymbol{\alpha}^i = U_i \tag{12}$$

with $U_i=(\tilde{u}(x_1^i)\ \tilde{u}(x_2^i)\dots\ \tilde{u}(x_{ni}^i))^t$. $\Phi_{\varepsilon_i,S_i}=(\Phi_{\varepsilon i}(x_j^i,x_k^i))_{1\le j,k\le n_i}$ is the local interpolation matrix and $\alpha^i=(\alpha_1^i,\alpha_2^i,\dots,\alpha_{n_i}^i)^t$.
The unknown coefficients α^i in (12) can be expressed in terms of the function values at the local interpolation points as

$$\boldsymbol{\alpha}^i = \Phi_{S_i,\varepsilon_i}^{-1} U_i. \tag{13}$$

The inverse matrix $\Phi_{S_i\varepsilon_i}^{-1}$ exists because of the positive definiteness of $\Phi_{S_i\varepsilon_i}$ [6]. Now, with the aim of obtaining a local discretized version for (7) consider $x_i\in\Omega\cap X$ or $X_i\in\partial\Omega\cap X$. In both cases a linear partial differential operator must be applied, either $\mathcal{L}$ or $\mathcal{B}$, to equation (11). For $x_i\in\Omega$ it follows

$$\begin{aligned} \mathcal{L}\mathcal{P}_{S_i,\varepsilon_i} u(\mathbf{x}_i) &= \sum_{j=1}^{n_i} \alpha_j^i \mathcal{L}\Phi_{\varepsilon_i}(\mathbf{x}_i,\mathbf{x}_j^i) \\ &= \mathcal{L}\Phi^1_{S_i,\varepsilon_i}\ \boldsymbol{\alpha}^i \\ &= \mathcal{L}\Phi^1_{S_i,\varepsilon_i}\Phi^{-1}_{S_i,\varepsilon_i} U_i \end{aligned} \tag{14}$$

where
$\mathcal{L}\ \Phi^{-1}_{S_i\varepsilon_i}=(\mathcal{L}\phi_{\varepsilon_i}(x_i^i,x_1^i)\dots\ \mathcal{L}\phi_{\varepsilon_i}(x_1^i,x_{n_i}^i))$.
Similarly, for $X_i\in\partial\Omega\cap X$

$$\mathcal{B}\mathcal{P}_{S_i,\varepsilon_i} u(\mathbf{x}_i) = \mathcal{B}\Phi^1_{S_i,\varepsilon_i}\Phi^{-1}_{S_i,\varepsilon_i} U_i. \tag{15}$$

We denote $\mathcal{L}_{S_i\varepsilon i}=\mathcal{L}\ \Phi^{-1}_{S_i\varepsilon_i}\Phi^{-1}_{S_i\varepsilon_i}$ and $\mathcal{B}_{S_i\varepsilon_i}=\mathcal{B}^1_{S_i\varepsilon_i}\Phi^{-1}_{S_i\varepsilon_i}$. From (14) and (15) it follows a discretized local version of (7)

$$\begin{aligned} &\mathcal{L}_{S_i,\varepsilon_i} U_i = f(\mathbf{x}_i), \ \text{for } \mathbf{x}_i\in\Omega\cap X, \\ &\mathcal{B}_{S_i,\varepsilon_i} U_i = g(\mathbf{x}_i), \ \text{for } \mathbf{x}_i\in\partial\Omega\cap X. \end{aligned}$$

The above system of linear equations can be assembled forming sparse matrix H of size $N \times N$ where the i–th row, associated to $x_i \in X$, has at most ni nonzero entries,and the unknown matrix is given by $U = \tilde{u}(x_1)\ \tilde{u}(x_2) \cdots \tilde{u}(x_N)$ (recall $x_i \equiv x_1^i$).

An approximated solution $\tilde{u}(x)$ at all the interpolation points can be obtained by solving $HU = F$. H can be considered a discretized version of the operator $\mathcal{L}$ including the boundary conditions involved in (7). The foregoing discussion gives rise to the following definition.

Definition 1. Let $\mathcal{L}: C^k(\Omega) \to C^{k-m}(\Omega)$ be a linear partial differential operator of order m, where $\Omega \subset \mathbb{R}^d$ is open and bounded. For $u \in C^k(\Omega)$ and $x \in \Omega$ consider an n–stencil $S_x = \{x_i\}_{i=1}^n \subset \Omega \cup \partial\Omega$ of nearest neighbors to x. Here $x_1 \equiv x$. The Gaussian RBF-FD operator associated to L denoted by $\mathcal{L}S_{x,\varepsilon}$ is defined by

$$\mathcal{L}_{S_{\mathbf{x}},\varepsilon} u(\mathbf{x}) = \mathcal{L}\Phi^1_{S_{\mathbf{x}},\varepsilon} \Phi^{-1}_{S_{\mathbf{x}},\varepsilon} U_{S_{\mathbf{x}}}, \tag{16}$$

where

$$\mathcal{L}\Phi^1_{S_{\mathbf{x}},\varepsilon} = \begin{pmatrix} \mathcal{L}\Phi_\varepsilon(\mathbf{y},\mathbf{x}_1)_{|\mathbf{y}=\mathbf{x}_1} & \mathcal{L}\Phi_\varepsilon(\mathbf{y},\mathbf{x}_2)_{|\mathbf{y}=\mathbf{x}_1} & \cdots & \mathcal{L}\Phi_\varepsilon(\mathbf{y},\mathbf{x}_n)_{|\mathbf{y}=\mathbf{x}_1} \end{pmatrix} \tag{17}$$

$$\Phi_{S_{\mathbf{x}},\varepsilon} = \begin{pmatrix} \Phi_\varepsilon(\mathbf{x}_1,\mathbf{x}_1) & \cdots & \Phi_\varepsilon(\mathbf{x}_1,\mathbf{x}_n) \\ \vdots & \ddots & \vdots \\ \Phi_\varepsilon(\mathbf{x}_n,\mathbf{x}_1) & \cdots & \Phi_\varepsilon(\mathbf{x}_n,\mathbf{x}_n) \end{pmatrix} \tag{18}$$

$$U_{S_{\mathbf{x}}} = \begin{pmatrix} u(\mathbf{x}_1) & u(\mathbf{x}_2) & \cdots & u(\mathbf{x}_n) \end{pmatrix}^t \tag{19}$$

and $\phi_\varepsilon(y;x_i) = e^{-\varepsilon^2}||y-x_i||^2$ with $\varepsilon > 0$. The Gaussian weights matrix of $\mathcal{L}$ at S_x is defined by

$$W\mathcal{L}_{S_{\mathbf{x}},\varepsilon} = \mathcal{L}\Phi^1_{S_{\mathbf{x}},\varepsilon} \Phi^{-1}_{S_{\mathbf{x}},\varepsilon}. \tag{20}$$

initially the application of Gaussian RBF-FD implies the solution of a small linear system at every node in order to compute weight matrices, a condition that increases the computational complexity of the problem. There are situations where the non-singular matrix $\Phi_{S_x,\varepsilon}$ is ill-conditioned, principally for small values of ε. In these events the RBF is near to the flat limit, however this issue has been overcome by using different methodologies resulting in stable calculations of (20), for example [10]-[12],[22], and recently [26] have used an hybrid kernel that is formed with two weighted terms, one Gaussian and another cubic which is given by $'\varphi(r) = \alpha e^{-(\varepsilon r)^2} + \beta r^3$,so this new hybrid kernel now involves three parameters.

Some RBF's do not contain a shape parameter ε. One well known example are polyharmonic splines $\varphi(r) = r^{2m} \log r, m \in \mathbb{N}$ and $\varphi(r) = r^{2m}; m \notin \mathbb{N}$. In general a RBF interpolator has the form

$$P_X u(\mathbf{x}) = \sum_{j=1}^{N} \alpha_j \phi(||\mathbf{x} - \mathbf{x}_j||) + p(\mathbf{x}),$$

where $p(x)$ is a low degree polynomial. The inclusion of $p(x)$, determines the invertibility of the interpolation matrix and this can be explained in terms of the theory of conditionally positive definite functions (for a wider perspective the reader may consult [34],[6]). For example polyharmonic splines include $p(x)$, while the gaussian function does not.

Up to now two kinds of RBF's have been applied in RBF-FD methods (i) infinitely smooth RBF's (which is the approach used in this paper) which contains a shape parameter. In this case is possible to get a high degree of accuracy in the solution although it is necessary to design strategies or algorithms for tuning the best value of the shape parameter and (ii) polyharmonic splines combined with the polynomial term RBF(PHS)- FD for short. This combination is free from a shape parameter but depends on the choice of PHS and polynomial degrees. $\phi(r)$ is less in uential but $p(x)$ cannot exceed a certain maximum, which increases with the local support size. Thus, the error estimates of RBF(PHS)-FD will depend on knowing the maximal permissible degree of supplementary polynomials (see Fornberg's book [8] for further information).

In this work, to obtain a relatively cheap solver, we focused on obtaining predictable weights with closed formulas depending on ε and h, ε will be adaptable according to the minimum local truncation error at position x. So we will be exploring within small stencils of node sets distributed on regular grids. The node density distribution may cause problems as to accuracy of the method. [8] discuss some methods in quasi-uniform node sets. In order to avoid point sets with sharp density differences we apply the algorithm from [30].

SHAPE PARAMETER FOR SOLUTIONS OF HELMHOLTZ EQUATION

For an homogeneous media the propagation of time-harmonic waves is modeled by Helmholtz equation with wavenumber $k = \omega c^{-1}$ where c is the sound speed and ω is the angular frequency. From the Fourier optics standpoint a time-harmonic wave can be seen as a superposition of plane waves and from the stationary phase method the timeharmonic wave field, at distant points, is due to a plane wave component; therefore it makes sense to consider planes waves as a key part of the analysis. Wave planes are a fundamental tool for investigating the behavior of numerical solutions for Helmholtz equation, either to reduce pollution effects or to design higher order discretizations, in this token, there are recent works such as [18] and [13].

Described below the method to obtain adequate shape parameters on general stencils for approximating a linear dierential operator $\mathcal{L}$ with smooth coefficients.

$$\mathcal{L} = \sum_{r,s} l_{rs}(\mathbf{x}) \partial_x^r \partial_y^s$$

when it is applied to solutions of Helmholtz equation. Let $p_{\mathcal{L}}(\xi,\eta) = \sum_{r,s} l_{r,s}(x)\ \xi^r \eta^s$ be the symbol of the linear differential operator $\mathcal{L}$ [37][2]. In particular consider plane waves given by $u(x;K,\xi\theta) = e^{ik(x\cos\theta + y\sin\theta)}$, therefore u satises

$$\mathcal{L}u(\mathbf{x};k,\theta) = p_{\mathcal{L}}(ik\cos\theta, ik\sin\theta) u(\mathbf{x};k,\theta). \tag{21}$$

Let $S = \{x_j\}_{j=1}^n$ be an n–stencil with respect to $x_1 = x = (x,y)$. The local truncation error by the approximation $\mathcal{L}_{S,\varepsilon} u(x;k;\theta)$ is given by

$$\begin{aligned} &\mathcal{L}u(\mathbf{x};k,\theta) - \mathcal{L}_{S,\varepsilon} u(\mathbf{x};k,\theta) \\ &= p_{\mathcal{L}}(ik\cos\theta, ik\sin\theta) u(\mathbf{x};k,\theta) - \mathcal{L}_{S,\varepsilon} u(\mathbf{x};k,\theta) \\ &= u(\mathbf{x};k,\theta)\left(p_{\mathcal{L}}(ik\cos\theta, ik\sin\theta) - \frac{1}{u(\mathbf{x};k,\theta)} \mathcal{L}\Phi^1_{S,\varepsilon} \Phi^{-1}_{S,\varepsilon} U_S\right) \\ &= u(\mathbf{x};k\ \theta)\left(p_{\mathcal{L}}(ik\cos\theta, ik\sin\theta) - \mathcal{L}\Phi^1_S\ \ \Phi^{-1}_S\, U_{S_0}\right) \end{aligned}$$

where $U_{S_0} = (u(x_1 - x; k; \theta)\cdots u(x_n - x; k; \theta))^t$. Note that

$$|\mathcal{L}u(\mathbf{x};k,\theta) - \mathcal{L}_{S,\varepsilon}u(\mathbf{x};k,\theta)| = |p_{\mathcal{L}}(ik\cos\theta, ik\sin\theta) - \mathcal{L}\Phi^{1}_{S,\varepsilon}\Phi^{-1}_{S,\varepsilon}U_{S_0}| \quad (22)$$

does not depend explicitly of x. We introduce the averaged local truncation error $\delta\mathcal{L}_s(\varepsilon, k)$ over all directions θ, by the integral

$$\delta\mathcal{L}_S(\varepsilon,k) = \frac{1}{2\pi}\int_0^{2\pi} |p_{\mathcal{L}}(ik\cos\theta, ik\sin\theta) - \mathcal{L}\Phi^{1}_{S,\varepsilon}\Phi^{-1}_{S,\varepsilon}U_{S_0}|d\theta. \quad (23)$$

From the last formula we choose the best shape parameter $\varepsilon_{\mathcal{L},S}(k)$, by

$$\varepsilon_{\mathcal{L},S}(k) = \arg\min_{\varepsilon>0} \delta\mathcal{L}_S(\varepsilon,k) \quad (24)$$

In particular, if $\mathcal{L} = \partial_x^r\partial_y^s$, then $p\mathcal{L}(ik\cos\theta; ik\sin\theta) = (ik)^{r+s}\cos^r\theta\sin^s\theta$. Also, since the symbol of Laplace operator is the polynomial $p\Delta(\xi,\eta) = \xi^2+\eta^2$, then $p\Delta(ik\cos\theta; ik\sin\theta) = -k^2$.

For implementations purposes, we approximated the integral (23) by means of Simpson's rule with $\Delta\theta = 2\pi/16$. To estimate the minimum argument (24) we used the Matlab function fminbnd.m, which use both Golden-section search and parabolic interpolation. This estimate requires roughly range between ten and twenty evaluations of (23). At each iteration, $\mathcal{L}\,\Phi^{-1}_{S,\varepsilon}\,\Phi^{-1}_{S,\varepsilon}$ is calculated once by Cholesky decomposition. With this procedure we try to reduce dispersion and pollution effects in numerical solutions of Helmholtz equation, calling this algorithm RBF-min.

DISPERSION ANALYSIS

Consider a solution u of Helmholtz equation $-\Delta u(x) - k^2u(x) = 0$. The classical dispersion analysis applies the relative phase error $|k-k_f|/k$

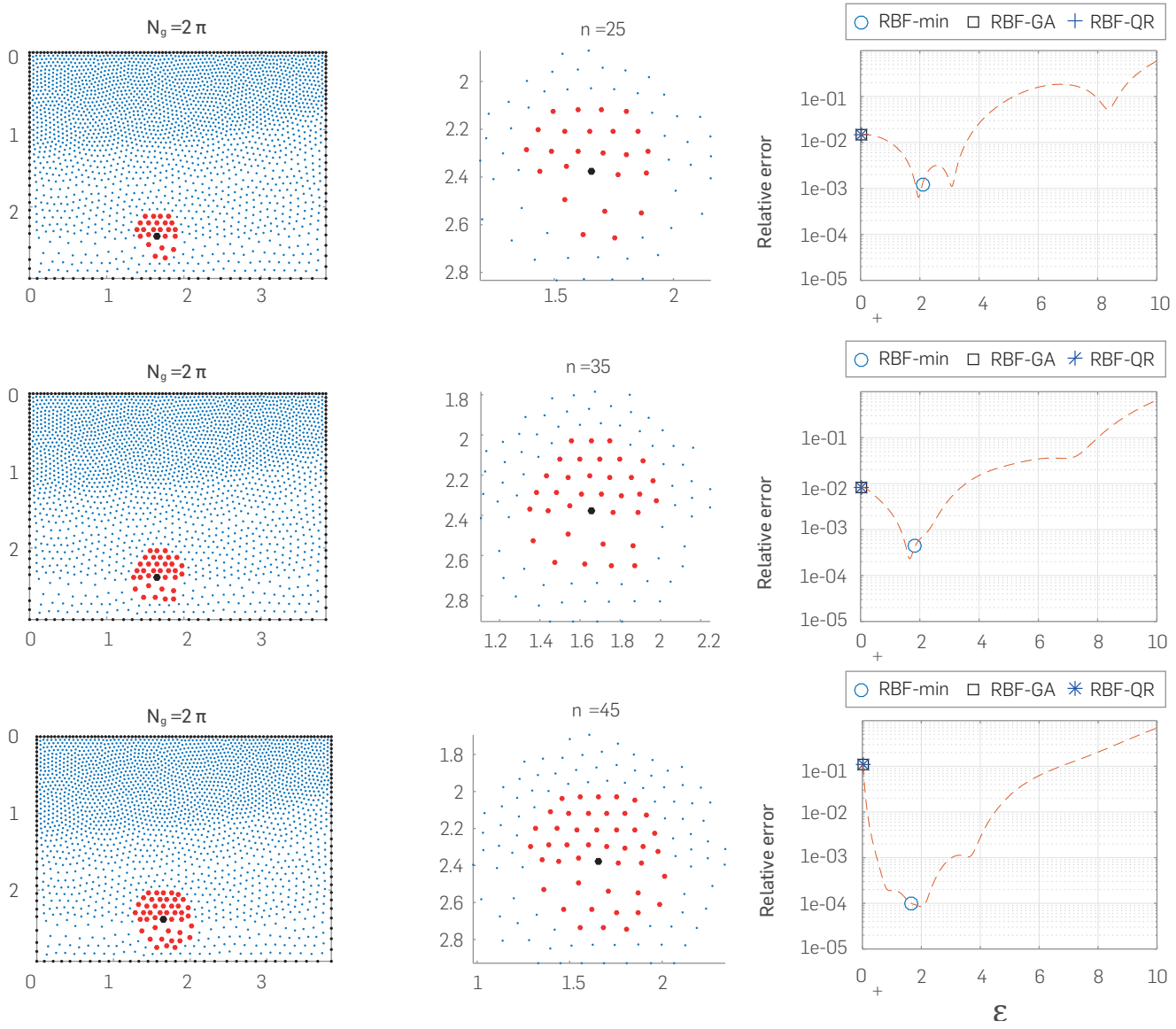

Figure 1 . Local truncation error approximating $\Delta u_1(x_c)$ for several stencil size. $u_1(x) = \frac{i}{4}H_0^{(1)}(k|x-xs|) + \frac{1}{15}u(x;k,\pi/4)$, in the figures Xc is the biggest point in black; at x_c, k = 9; 56 and Xs = (3:5; 0:5). Node distribution is based on a region of the smooth Marmousi model.

where k_f is the wavenumber of the numerical solution, which locally satises

$$-\Delta_{S,\varepsilon}u(\mathbf{x}) - k_f^2 u(\mathbf{x}) = 0. \tag{25}$$

The occurrence of the fictitious wavenumber k_f is known as numerical dispersion and can be studied by the phase lag $|k\text{-}k_f|$. However, as the solution of the Helmholtz equation fluctuates considerably for large wavenumbers the situation is even worse because for measuring the properties of a finite difference scheme, considering only the convergence order is not enough. In fact, the accuracy of the numerical solution deteriorates with increasing wavenumber k even when the resolution factor kh, is kept constant. This phenomenon is related to the so-called 'pollution effect' (see, [17]). Therefore our next task is to build an strategy to mitigate this phenomenon.

To obtain an explicit relation between k and k_f we consider the plane wave

$$u(x, y; k, \theta) = e^{ik((\cos\theta)x+(\sin\theta)y)}$$

with propagation angle θ and wave length $\lambda=2\pi/k$. According to (25) we can take k_f as a function which depends on k, θ the stencil S and ε, given by its square

$$k_f^2(k, \theta, \varepsilon) = -\frac{\Delta_{S,\varepsilon}u(x, y; k, \theta)}{u(x, y, k, \theta)}. \tag{26}$$

Note that the local truncation error (22) for $\mathcal{L}=\Delta$ is given just by

$$|\Delta u(\mathbf{x}; k, \theta) - \Delta_{S,\varepsilon}u(\mathbf{x}; k, \theta)| = |k^2 - k_f^2(k, \theta, \varepsilon)|, \tag{27}$$

The fictitious wavenumber is anisotropic, i.e., it depends on the wave propagation direction θ. As was the case in [27], our objective will be to choose the shape parameter ε such that the average phase error, over all angles of propagation, is minimum. Hence in minimizing the averaged local truncation error

$$\delta\Delta_S(\varepsilon, k) = \frac{1}{2\pi}\int_0^{2\pi} |k^2 - \Delta\Phi_{S,\varepsilon}^1\Phi_{S,\varepsilon}^{-1}U_{S_0}|d\theta \tag{28}$$

for the variable ε we can mitigate the pollution effect due to dispersion error

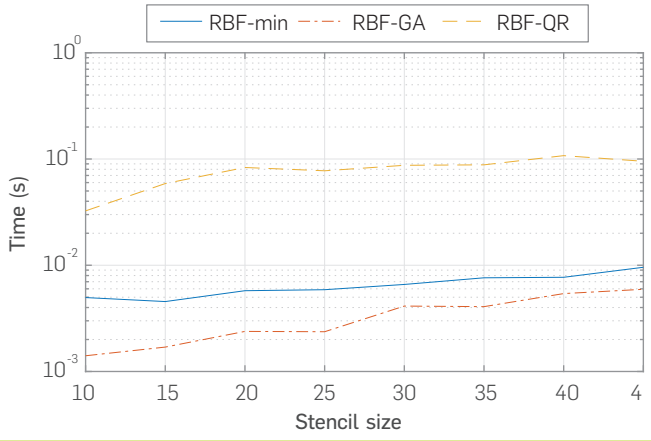

Figure 2 . Comparison of runtime in calculations of stable weights of results presented in Figure. 1.

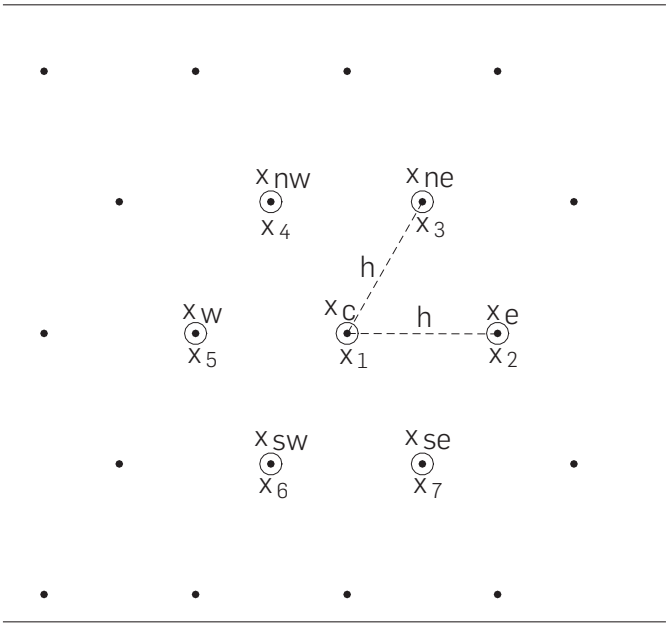

Figure 3 . 7−stencil on a regular hexagonal grid.

SOME CLOSED FORMULAS AND TRUNCATION ERROR

In the context of numerical solutions of the wave equation, numerical stability and isotropy are enhanced with a similar computational work when compared with the standard numerical methods in the simulation of heterogeneous and random media. For example, whereas Von Neumann stability in solution of the 2D acoustic wave equation by explicit finite differences with 5−points needs to satisfy the estimate $\frac{\Delta t}{\Delta x} \leq c^{-1}\frac{\sqrt{2}}{2}$, with hexagonal 7−stencil, this estimate is improved to $\frac{\Delta t}{\Delta x} \leq c^{-1}\frac{\sqrt{2}}{\sqrt{3}}$ [7]. Besides, with hexagonal stencils we have reached similar results to those reported in [3] where the authors have developed an optimal Cartesian 9−stencil for Helmholtz equation with the goal of mitigating the pollution effect.

We start considering the 7−stencil $\mathrm{H} = [x_i]_{i=1}^7$, built on an hexagonal regular grid as in **Figure 3**. For $h > 0$ and $x_1 = (x; y)$ as central node, the coordinates of the other points in H are given by

$$\mathbf{x}_2 = (x + h, y),\ \mathbf{x}_3 = (x + h/2, y + \sqrt{3}h/2),$$
$$\mathbf{x}_4 = (x - h/2, y + \sqrt{3}h/2),\ \mathbf{x}_5 = (x - h, y),$$
$$\mathbf{x}_6 = (x - h/2, y - \sqrt{3}h/2),\ \mathbf{x}_7 = (x + h/2, y - \sqrt{3}h/2)$$

Sometimes will be convenient to work with subscripts referred by cardinal directions:

$$\mathbf{x}_c = \mathbf{x}_1,\ \mathbf{x}_\mathbf{e} = \mathbf{x}_2,\ \mathbf{x}_\mathbf{ne} = \mathbf{x}_3,\ \mathbf{x}_\mathbf{nw} = \mathbf{x}_4,$$
$$\mathbf{x}_\mathbf{w} = \mathbf{x}_5,\ \mathbf{x}_\mathbf{sw} = \mathbf{x}_5,\ \mathbf{x}_\mathbf{se} = \mathbf{x}_7$$

With the given labeled order in the 7−stencil H and with $p = e^{-(\varepsilon h)2}$, the interpolation matrix $\Phi_{H,\varepsilon}$ is explicitly given by

$$\Phi_{H,\varepsilon}=\begin{pmatrix} 1 & p & p & p & p & p & p \\ p & 1 & p & p^3 & p^4 & p^3 & p \\ p & p & 1 & p & p^3 & p^4 & p^3 \\ p & p^3 & p & 1 & p & p^3 & p^4 \\ p & p^4 & p^3 & p & 1 & p & p^3 \\ p & p^3 & p^4 & p^3 & p & 1 & p \\ p & p & p^3 & p^4 & p^3 & p & 1 \end{pmatrix}. \tag{29}$$

From this formula, we seek expressions for $(\partial_x)_{H,\varepsilon}$, $(\partial_y)_{H,\varepsilon}$, $(\partial_x^2)_{H,\varepsilon}$, $(\partial_y^2)_{H,\varepsilon}$, $(\partial_{xy})_{H,\varepsilon}$ and $\Delta_{H,\varepsilon}$ applied at $u(x_1)$. Using a software of symbolic calculus we obtain

$$\begin{aligned}
\partial_x\Phi^1_{H,\varepsilon}\Phi^{-1}_{H,\varepsilon} &= D(h,\varepsilon)\begin{pmatrix} 0 & 2 & 1 & -1 & -2 & -1 & 1 \end{pmatrix} \\
\partial_y\Phi^1_{H,\varepsilon}\Phi^{-1}_{H,\varepsilon} &= \sqrt{3}D(h,\varepsilon)\begin{pmatrix} 0 & 0 & 1 & 1 & 0 & -1 & -1 \end{pmatrix} \\
\partial_x^2\Phi^1_{H,\varepsilon}\Phi^{-1}_{H,\varepsilon} &= F_1(h,\varepsilon)\begin{pmatrix} 0 & 1 & 0 & 0 & 1 & 0 & 0 \end{pmatrix} \\
&\quad + G_1(h,\varepsilon)\begin{pmatrix} 0 & 0 & 1 & 1 & 0 & 1 & 1 \end{pmatrix} \\
&\quad -2E(h,\varepsilon)\begin{pmatrix} 1 & 0 & 0 & 0 & 0 & 0 & 0 \end{pmatrix} \\
\partial_x^2\Phi^1_{H,\varepsilon}\Phi^{-1}_{H,\varepsilon} &= F_2(h,\varepsilon)\begin{pmatrix} 0 & 1 & 0 & 0 & 1 & 0 & 0 \end{pmatrix} \\
&\quad + G_2(h,\varepsilon)\begin{pmatrix} 0 & 0 & 1 & 1 & 0 & 1 & 1 \end{pmatrix} \\
&\quad -2E(h,\varepsilon)\begin{pmatrix} 1 & 0 & 0 & 0 & 0 & 0 & 0 \end{pmatrix} \\
\partial_{xy}\Phi^1_{H,\varepsilon}\Phi^{-1}_{H,\varepsilon} &= \frac{\sqrt{3}}{2}F_3(h,\varepsilon)\begin{pmatrix} 0 & 0 & 1 & -1 & 0 & 1 & -1 \end{pmatrix}
\end{aligned} \tag{30}$$

where

$$D(h,\varepsilon)=\frac{h\varepsilon^2\left(\coth\left(h^2\varepsilon^2\right)+1\right)}{4\cosh\left(h^2\varepsilon^2\right)+2}$$

$$E(h,\varepsilon)=\frac{3h^2\varepsilon^4}{2\cosh\left(h^2\varepsilon^2\right)+\cosh\left(2h^2\varepsilon^2\right)-3}+\varepsilon^2$$

$$F_1(h,\varepsilon)=\frac{h^2\varepsilon^4e^{h^2\varepsilon^2}\left(4\cosh\left(h^2\varepsilon^2\right)+5\right)\operatorname{csch}^2\left(\frac{h^2\varepsilon^2}{2}\right)}{4\left(5\cosh\left(h^2\varepsilon^2\right)+\cosh\left(2h^2\varepsilon^2\right)+3\right)}$$

$$G_1(h,\varepsilon)=\frac{h^2\varepsilon^4e^{h^2\varepsilon^2}}{2\left(5\cosh\left(h^2\varepsilon^2\right)+\cosh\left(2h^2\varepsilon^2\right)+3\right)} \tag{31}$$

$$F_2(h,\varepsilon)=-\frac{3h^2\varepsilon^4e^{h^2\varepsilon^2}\operatorname{csch}^2\left(\frac{h^2\varepsilon^2}{2}\right)}{4\left(5\cosh\left(h^2\varepsilon^2\right)+\cosh\left(2h^2\varepsilon^2\right)+3\right)}$$

$$G_2(h,\varepsilon)=\frac{3h^2\varepsilon^4\left(e^{h^2\varepsilon^2}+1\right)^2\operatorname{csch}^2\left(\frac{h^2\varepsilon^2}{2}\right)}{8\left(5\cosh\left(h^2\varepsilon^2\right)+\cosh\left(2h^2\varepsilon^2\right)+3\right)}$$

$$F_3(h,\varepsilon)=\frac{h^2\varepsilon^4e^{h^2\varepsilon^2}\operatorname{csch}^2\left(\frac{h^2\varepsilon^2}{2}\right)}{4\cosh\left(h^2\varepsilon^2\right)+2}$$

Also, we note that $F_1+F_2=G_1+G_2$ and denote it by $F=F_1+F_2=G_1+G_2$, explicitly

$$F(h,\varepsilon)=\frac{h^2\varepsilon^4e^{h^2\varepsilon^2}\operatorname{csch}^2\left(\frac{h^2\varepsilon^2}{2}\right)}{2\cosh\left(h^2\varepsilon^2\right)+4} \tag{32}$$

Formulas for partial derivative operators of second order. By simple substitutions with the group of equations (31) within of equations in (30) we have explicit formulas for approximating partial derivative operators of second order

$$\begin{aligned}
&(\partial_x)_{H,\varepsilon}u(\mathbf{x_c}) = \\
&\quad D(h,\varepsilon)(2u_2+u_3-u_4-2u_5-u_6+u_7) \\
&(\partial_y)_{H,\varepsilon}u(\mathbf{x_c}) = \\
&\quad \sqrt{3}D(h,\varepsilon)(u_3+u_4-u_6-u_7) \\
&(\partial_x^2)_{H,\varepsilon}u(\mathbf{x_c}) = \\
&\quad -2E(h,\varepsilon)u_1+F_1(h,\varepsilon)(u_2+u_5) \\
&\quad +G_1(h,\varepsilon)(u_3+u_4+u_6+u_7) \\
&(\partial_y^2)_{H,\varepsilon}u(\mathbf{x_c}) = \\
&\quad -2E(h,\varepsilon)u_1+F_2(h,\varepsilon)(u_2+u_5) \\
&\quad +G_2(h,\varepsilon)(u_3+u_4+u_6+u_7) \\
&(\partial_{xy})_{H,\varepsilon}u(\mathbf{x}_c) = \\
&\quad \tfrac{\sqrt{3}}{2}F_3(h,\varepsilon)(u_3-u_4+u_6-u_7) \\
&\Delta_{H,\varepsilon}u(\mathbf{x}_c) = \\
&\quad -4E(h,\varepsilon)u_1+F(h,\varepsilon)(u_2+u_3+u_4+u_5+u_6+u_7)
\end{aligned} \tag{33}$$

As it is usual in finite differences schemes, once an approximation is proposed, the first step is to investigate its local truncation error. The standard methodology consists in making comparisons with Taylor polynomials. The next lemma will be useful in that sense.

Lemma 1. For $0<\varepsilon h<\sqrt{\frac{\pi}{2}}$ the following approximations of weights functions in (31) hold

$$\begin{aligned}
D(h,\varepsilon) &= \tfrac{1}{6h}+\tfrac{h\varepsilon^2}{6}+\mathcal{O}(\varepsilon^3h^4) \\
E(h,\varepsilon) &= \tfrac{1}{h^2}+\varepsilon^2-\tfrac{h^2\varepsilon^4}{4}+\mathcal{O}(\varepsilon^6h^4) \\
F_1(h,\varepsilon) &= \tfrac{1}{h^2}+\varepsilon^2+\tfrac{5h^2\varepsilon^4}{36}+\mathcal{O}(\varepsilon^6h^4) \\
G_1(h,\varepsilon) &= \tfrac{h^2\varepsilon^4}{18}+\tfrac{h^4\varepsilon^6}{18}+\mathcal{O}(\varepsilon^8h^6) \\
F_2(h,\varepsilon) &= -\tfrac{1}{3h^2}-\tfrac{\varepsilon^2}{3}+\tfrac{h^2\varepsilon^4}{36}+\mathcal{O}(\varepsilon^6h^4) \\
G_2(h,\varepsilon) &= \tfrac{2}{3h^2}+\tfrac{2\varepsilon^2}{3}+\tfrac{h^2\varepsilon^4}{9}+\mathcal{O}(\varepsilon^6h^4) \\
F_3(h,\varepsilon) &= \tfrac{2}{3h^2}+\tfrac{2\varepsilon^2}{3}+\tfrac{h^2\varepsilon^4}{18}+\mathcal{O}(\varepsilon^6h^4) \\
F(h,\varepsilon) &= \tfrac{2}{3h^2}+\tfrac{2\varepsilon^2}{3}+\tfrac{h^2\varepsilon^4}{6}+\mathcal{O}(\varepsilon^6h^4).
\end{aligned} \tag{34}$$

One way to test the quality of the method is to point out the relationship with other finite difference schemes. It is not difficult to show that the standard finite difference method is the limit of the RBF-FD scheme, it occurs when the width of the Gaussian RBF, controlled by the shape parameter ε, tends to be at.

Remark 1. By examining the limit situation $\varepsilon\to 0^+$ with $\Delta_{H,\varepsilon}u(Xc)$ in (33) via approxi-mations in (34) we recover the formula

$$\Delta_{H,0^+}u(\mathbf{x_c})=-\frac{4}{h^2}u_{\mathbf{c}}+\frac{2}{3h^2}\left(u_{\mathbf{e}}+u_{\mathbf{ne}}+u_{\mathbf{nw}}+u_{\mathbf{w}}+u_{\mathbf{sw}}+u_{\mathbf{se}}\right). \tag{35}$$

given in [7], corresponding to the standard finite difference formulation derived by Taylor expansions.

Local truncation errors. To estimate the local truncation error of the approximations $\mathcal{L}_{H,\varepsilon}u(x) \approx \mathcal{L}u(x)$ it suffices to expand $u(x_i)$, for $i = 2, 3; ..., 7$, in Taylor polynomials around $x_1 = x_c$, and then substituting them in (33), obtaining

$$
\begin{aligned}
&(\partial_x)_{H,\varepsilon}u(\mathbf{x}_1)\\
&\quad = 6hD(h,\varepsilon)\partial_x u(\mathbf{x}_1) + \tfrac{1}{4}D(h,\varepsilon)\left(3h^3(\partial_x^3 u(\mathbf{x}_1)\right.\\
&\quad \left. + \partial_x\partial_y^2 u(\mathbf{x}_1)) + \mathcal{O}(h^4)\right)\\
&(\partial_y)_{H,\varepsilon}u(\mathbf{x}_1)\\
&\quad = 6hD(h,\varepsilon)\partial_y u(\mathbf{x}_1) + \tfrac{1}{4}D(h,\varepsilon)\left(3h^3(\partial_y^3 u(\mathbf{x}_1)\right.\\
&\quad \left. + \partial_y\partial_x^2 u(\mathbf{x}_1)) + \mathcal{O}(h^4)\right)\\
&(\partial_x^2)_{H,\varepsilon}u(\mathbf{x}_1)\\
&\quad = \tfrac{h^2}{2}(2F_1(h,\varepsilon) + G_1(h,\varepsilon))\partial_x^2 u(\mathbf{x}_1) + (2F_1(h,\varepsilon)\\
&\quad + 4G_1(h,\varepsilon) - 2E(h,\varepsilon))\,u(\mathbf{x}_1)\\
&\quad + \tfrac{3}{2}h^2 G_1(h,\varepsilon)\partial_y^2 u(\mathbf{x}_1) + F(h,\varepsilon)\mathcal{O}(h^4) \qquad (36)\\
&(\partial_y^2)_{H,\varepsilon}u(\mathbf{x}_1)\\
&\quad = \tfrac{h^2}{2}(2F_2(h,\varepsilon) + G_2(h,\varepsilon))\partial_x^2 u(\mathbf{x}_1) + (2F_2(h,\varepsilon)\\
&\quad + 4G_2(h,\varepsilon) - 2E(h,\varepsilon))\,u(\mathbf{x}_1)\\
&\quad + \tfrac{3}{2}h^2 G_2(h,\varepsilon)\partial_y^2 u(\mathbf{x}_1) + F(h,\varepsilon)\mathcal{O}(h^4)\\
&(\partial_{xy})_{H,\varepsilon}u(\mathbf{x}_1)\\
&\quad = \tfrac{3}{2}h^2 F_3(h,\varepsilon)\partial_{xy}u(\mathbf{x}_1) + F_3(h,\varepsilon)\mathcal{O}(h^4)\\
&\quad \Delta_{H,\varepsilon}u(\mathbf{x}_1) = \tfrac{3}{2}h^2 F(h,\varepsilon)\Delta u(\mathbf{x}_1) + (6F(h,\varepsilon)\\
&\quad - 4E(h,\varepsilon))\,u(\mathbf{x}_1) + 2F(h,\varepsilon)\mathcal{O}(h^4)
\end{aligned}
$$

From Taylor polynomials in (34) the following error can be obtained

$$
\begin{aligned}
|6hD(h,\varepsilon) - 1| &\le h^2\varepsilon^2\\
\left|\tfrac{h^2}{2}(2F_1(h,\varepsilon) + G_1(h,\varepsilon)) - 1\right| &\le h^2\varepsilon^2 + \tfrac{h^4\varepsilon^4}{6}\\
|2F_1(h,\varepsilon) + 4G_1(h,\varepsilon) - 2E(h,\varepsilon)| &\le h^2\varepsilon^4\\
\left|\tfrac{3}{2}h^2 G_1(h,\varepsilon)\right| &\le \tfrac{h^4\varepsilon^4}{12} + \tfrac{h^6\varepsilon^6}{12}\\
\left|\tfrac{h^2}{2}(2F_2(h,\varepsilon) + G_2(h,\varepsilon))\right| &\le \tfrac{h^4\varepsilon^4}{12} + \tfrac{h^6\varepsilon^6}{12} \qquad (37)\\
\left|\tfrac{3}{2}h^2 G_2(h,\varepsilon) - 1\right| &\le h^2\varepsilon^2 + \tfrac{h^4\varepsilon^4}{6}\\
|2F_2(h,\varepsilon) + 4G_2(h,\varepsilon) - 2E(h,\varepsilon)| &\le h^2\varepsilon^4\\
\left|\tfrac{3}{2}h^2 F(h,\varepsilon) - 1\right| &\le h^2\varepsilon^2 + \tfrac{h^4\varepsilon^4}{4}\\
|6F(h,\varepsilon) - 4E(h,\varepsilon)| &\le 2h^2\varepsilon^4\\
\left|\tfrac{3}{2}h^2 F_3(h,\varepsilon) - 1\right| &\le h^2\varepsilon^2 + \tfrac{h^4\varepsilon^4}{12}
\end{aligned}
$$

from which the error estimates can be obtained for (33) with their respective approximation errors

$$
\begin{aligned}
|(\partial_x)_{H,\varepsilon}u(\mathbf{x}) - \partial_x u(\mathbf{x})| &\le h^2\varepsilon^2|\partial_x u(\mathbf{x})| + \mathcal{O}(\varepsilon^2h^2)\\
|(\partial_y)_{H,\varepsilon}u(\mathbf{x}) - \partial_y u(\mathbf{x})| &\le h^2\varepsilon^2|\partial_y u(\mathbf{x})| + \mathcal{O}(\varepsilon^2h^2)\\
|(\partial_x^2)_{H,\varepsilon}u(\mathbf{x}) - \partial_x^2 u(\mathbf{x})| &\le \left(h^2\varepsilon^2 + \tfrac{h^4\varepsilon^4}{6}\right)|\partial_x^2 u(\mathbf{x})|\\
&\quad + \left(\tfrac{h^4\varepsilon^4}{12} + \tfrac{h^6\varepsilon^6}{12}\right)|\partial_y^2 u(\mathbf{x})|\\
&\quad + h^2\varepsilon^4|u(\mathbf{x})| + \mathcal{O}(\varepsilon^2h^2)\\
|(\partial_y^2)_{H,\varepsilon}u(\mathbf{x}) - \partial_y^2 u(\mathbf{x})| &\le \left(\tfrac{h^4\varepsilon^4}{12} + \tfrac{h^6\varepsilon^6}{12}\right)|\partial_x^2 u(\mathbf{x})| \qquad (38)\\
&\quad + \left(h^2\varepsilon^2 + \tfrac{h^4\varepsilon^4}{6}\right)|\partial_y^2 u(\mathbf{x})|\\
&\quad + h^2\varepsilon^4|u(\mathbf{x})| + \mathcal{O}(\varepsilon^2h^2)\\
|(\partial_{xy})_{H,\varepsilon}u(\mathbf{x}) - \partial_{xy}u(\mathbf{x})| &\le h^2\varepsilon^2|\partial_{xy}u(\mathbf{x})| + \mathcal{O}(\varepsilon^2h^2)\\
|\Delta_{H,\varepsilon}u(\mathbf{x}) - \Delta u(\mathbf{x})| &\le \left(h^2\varepsilon^2 + \tfrac{h^4\varepsilon^4}{4}\right)|\Delta u(\mathbf{x})|\\
&\quad + 2h^2\varepsilon^4|u(\mathbf{x})| + \mathcal{O}(\varepsilon^2h^2).
\end{aligned}
$$

The above treatment and discussion can be summarized in the next result

Theorem 1. Let u be a function in $C^4(\Omega)$ with $\Omega\subset\mathbb{R}^2$ a convex open set. Then for $x \in\Omega$, $h > 0$ small enough such that $H\subset \Omega$ and $\varepsilon>0$ such that $0 < \varepsilon h <\sqrt{\frac{\pi}{2}}$; the following assertions about the Gaussian RBF-FD approximations hold:

- $(\partial_x)_{H\varepsilon}u(x)= \partial_x u(x) + \mathcal{O}(\varepsilon^2h^2)$
- $(\partial_y)_{H\varepsilon}u(x)= \partial_y u(x) + \mathcal{O}(\varepsilon^2h^2)$
- $(\partial_x^2)_{H\varepsilon}u(x)= \partial_x^2 u(x) + \mathcal{O}(\varepsilon^2h^2)$
- $(\partial_y^2)_{H\varepsilon}u(x)= \partial_y^2 u(x) + \mathcal{O}(\varepsilon^2h^2)$
- $(\partial_{xy})_{H\varepsilon}u(x)= \partial_{xy} u(x) + \mathcal{O}(\varepsilon^2h^2)$
- $\Delta_{H\varepsilon}u(x)= \Delta^2 u(x) + \mathcal{O}(\varepsilon^2h^2)$

In **Figure 4** it is depicted a comparison of RBF-FD with 5–stencils and 7–stencils against its respective standard finite differences approximations. To conduct this test we chose the Hankel function of the rst kind $u(x)=H_0^{(1)}(k|\mathbf{x}|)$ with $k = 100$ and $h = 0{:}01$. We can observe the behaviour of the relative truncation error

$$
\frac{|\partial_x H_0^{(1)}(k|\mathbf{x}_1|) - (\partial_x)_{H\varepsilon}H_0^{(1)}(k|\mathbf{x}_1|)|}{|\partial_x H_0^{(1)}(k|\mathbf{x}_1|)|} \ (\text{figure 4-}\textit{left}) \qquad (39)
$$

and

$$
\frac{|\Delta H_0^{(1)}(k|\mathbf{x}_1|) - \Delta_{H,\varepsilon}H_0^{(1)}(k|\mathbf{x}_1|)|}{|\Delta H_0^{(1)}(k|\mathbf{x}_1|)|} \ (\text{figure 4-}\textit{right}). \qquad (40)
$$

It is worth to point out that in both situations there exist values of ε where the error reaches a minimum value. Furthermore it confirms that the limit situation $\varepsilon\to 0^+$, RBF-FD coincides with FD.

OPTIMAL SHAPE PARAMETER ON HEXAGONAL STENCIL

We derive closed formulas to rapidly obtain the optimal shape parameter in the context of hexagonal stencils.

Remark 2. Let u be a solution of the Helmholtz equation. By theorem 1.

$$\Delta_{H,\varepsilon}u(x,y) = \Delta u(x,y) + \mathcal{O}(\varepsilon^2 h^2)$$

for any $\varepsilon > 0$ on a hexagonal stencil H of size h centered at $(x; y)$, we have that for small enough h

$$\Delta_{H,\varepsilon}u(x,y) + k^2 u(x,y) = \mathcal{O}(\varepsilon^2 h^2) \tag{41}$$

In this case the ctitious wavenumber k_f depends also of the stencil size h, so $k_f = k_f(k;\theta; h; \varepsilon)$ is such that

$$\Delta_{H,\varepsilon}u(x,y) + k_f^2 u(x,y) = 0. \tag{42}$$

As we have already seen, k_f is related to the truncation error of the Laplace operator applied in u by $(k^2 - k_f^2)u(x, y) = \mathcal{O}(\varepsilon^2 h^2)$.

In this case, thanks to the symmetry of the hexagonal stencil, it is possible to nd an explicit relation between k and kf . From (33) in (26) we obtain the formula

$$k_f^2(k,\theta,h,\varepsilon) = 4E(h,\varepsilon) - 2F(h,\varepsilon)T(k,\theta,h) \tag{43}$$

where

$$T(k,\theta,h) = \cos(hk\cos\theta) + 2\cos\left(\frac{1}{2}hk\cos\theta\right)\cos\left(\frac{\sqrt{3}}{2}hk\sin\theta\right). \tag{44}$$

In **Figure 5 (left)** there is a plot of the residual $|\delta k(k,\theta,h,\varepsilon)| = |k^2 - k_f^2(k, \theta, h\ \varepsilon)|$ where it can appreciated that for some values of ε it is possible to have good accuracy even in scaling h for keeping $hk = 1$ or equivalently $h = \frac{\lambda}{2\pi}$, that is, by fixing $2\pi \approx 6$ points per wavelength. Next lemma will allow us to introduce a simplified variant of (43) which does not depend of θ, by just taking the mean value over $[0,2\pi]$.

Lemma 2. For any $(h,k) \in \mathbb{R}^2$, T as in (44) satises the equality

$$\int_0^{2\pi} T(k,\theta,h)d\theta = 6\pi J_0(hk), \tag{45}$$

where J_0 is the Bessel function of first kind.
Proof. First, note that $T(k,\theta + \frac{\pi}{3},h) = T(k,\theta, h)$, thus T has period $\frac{\pi}{3}$ in the second argument and

$$\int_0^{2\pi} T(k,\theta,h)d\theta = 6\int_0^{\pi/3} T(k,\theta,h)d\theta, \tag{46}$$

then, considering the identity

$$2\cos\left(\frac{1}{2}hk\cos(\theta)\right)\cos\left(\frac{\sqrt{3}}{2}hk\sin(\theta)\right) = \cos\left(hk\cos\left(\theta + \frac{\pi}{3}\right)\right) + \cos\left(hk\cos\left(\theta - \frac{\pi}{3}\right)\right) \tag{47}$$

and by a few changes of variable we can finally obtain

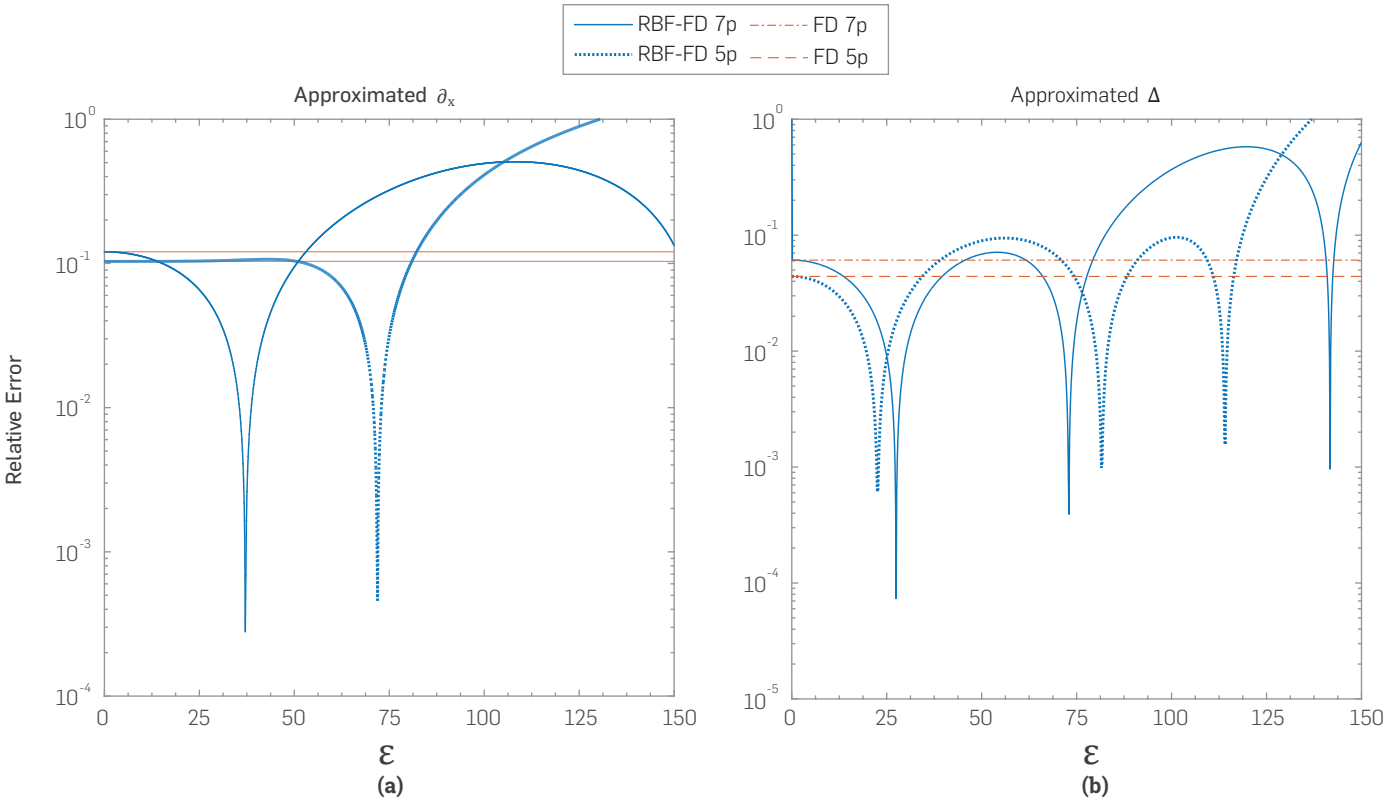

Figure 4 . Plot of relative error (left) (39) and (right) (40) with x1 = (2; 1:5), k = 100 and h = 0:01 is the stencil size.

$$\begin{aligned}
&\int_0^{\pi/3} T(k,\theta,h)d\theta \\
&= \int_0^{\pi/3} \cos(hk\cos\theta)d\theta + \int_0^{\pi/3} \cos\left(hk\cos\left(\theta+\frac{\pi}{3}\right)\right)d\theta \\
&\quad + \int_0^{\pi/3} \cos\left(hk\cos\left(\theta-\frac{\pi}{3}\right)\right)d\theta \\
&= \int_0^{\pi/3} \cos(hk\cos\theta)d\theta + \int_{\pi/3}^{2\pi/3} \cos(hk\cos\theta)d\theta \\
&\quad + \int_{2\pi/3}^{\pi} \cos(hk\cos\theta)d\theta \\
&= \int_0^{\pi} \cos(hk\cos\theta)d\theta \\
&= \pi J_0(hk)
\end{aligned}$$

where the last equality is a well known integral representation of the Bessel functions. We define $\widetilde{k}_f$ such that

$$\widetilde{k}_f^2(k,h,\varepsilon) = \frac{1}{2\pi}\int_0^{2\pi} k_f^2(k,\theta,h,\varepsilon)d\theta \tag{48}$$

explicitly results in the formula

$$\widetilde{k}_f^2(k,h,\varepsilon) = 4E(h,\varepsilon) - 6F(h,\varepsilon)J_0(hk), \tag{49}$$

and we also introduced a new residual function $\delta\widetilde{k}(k,h,\varepsilon)$. We will see later what is the error between $k_f(k,h,\varepsilon)$ and $\widetilde{k}_f(k,h,\varepsilon)$ and $\widetilde{k}_f(k,h,\varepsilon)$ produced by "neglecting" θ in taking the mean value (48).

Lemma 3. Let h and k be positive real numbers with small enough h, then

$$\begin{aligned}
&\lim_{\varepsilon\to 0^+} \delta\widetilde{k}(k,h,\varepsilon) \\
&= \frac{h^2k^2 + 4J_0(hk) - 4}{h^2} > 0 \; and \; \lim_{\varepsilon\to\infty} \delta\widetilde{k}(k,h,\varepsilon) = -\infty
\end{aligned} \tag{50}$$

Proof. By supposing $0 < \varepsilon h < \sqrt{\frac{\pi}{2}}$, using the expansions in (34) at (49) and taking $\varepsilon \to 0^+$, then $\lim_{\varepsilon\to 0^+} \delta\widetilde{k}(k,h,\varepsilon) = \frac{h^2k^2+4J0(hk)-4}{h^2}$. From the Taylor series of J_0 it is true that

$$J_0(hk) > 1 - \frac{h^2k^2}{4},$$

and the inequality is thus obtained. For the second limit note that from the explicit formula for (49) given by

$$\begin{aligned}
\delta\widetilde{k}(k,h,\varepsilon) &= k^2 - 4\varepsilon^2\left(\frac{3h^2\varepsilon^2}{2\cosh(h^2\varepsilon^2)+\cosh(2h^2\varepsilon^2)-3}+1\right) \\
&+ 3\varepsilon^2\frac{h^2\varepsilon^2 e^{h^2\varepsilon^2}\operatorname{csch}^2\left(\frac{h^2\varepsilon^2}{2}\right)}{\cosh(h^2\varepsilon^2)+2}J_0(hk),
\end{aligned}$$

we can see that

$$\begin{aligned}
\delta\widetilde{k}(0,1,\varepsilon) &= -4\varepsilon^2\left(\frac{3\varepsilon^2}{2\cosh(\varepsilon^2)+\cosh(2\varepsilon^2)-3}+1\right) \\
&\quad + 3\varepsilon^2\frac{\varepsilon^2 e^{\varepsilon^2}\operatorname{csch}^2\left(\frac{\varepsilon^2}{2}\right)}{\cosh(\varepsilon^2)+2} \\
&= -4\varepsilon^2 + 6\varepsilon^4\frac{\coth\left(\frac{\varepsilon^2}{2}\right)+1}{\cosh(\varepsilon^2)+2}
\end{aligned}$$

In addition, can be observed above that the behavior of $\delta\widetilde{k}(k,h,\varepsilon)$ and $\delta\widetilde{k}(0,1,\varepsilon)$ when $\varepsilon \to \infty$ are the same, hence

$$\begin{aligned}
\lim_{\varepsilon\to\infty}\delta\widetilde{k}(k,h,\varepsilon) &= \lim_{\varepsilon\to\infty}\delta\widetilde{k}(0,1,\varepsilon) \\
&= \lim_{\varepsilon\to\infty}\left(-4\varepsilon^2 + 6\varepsilon^4\frac{\coth\left(\frac{\varepsilon^2}{2}\right)+1}{\cosh(\varepsilon^2)+2}\right) \\
&= -\infty.
\end{aligned}$$

The above lemma and the continuity of the function $\delta\widetilde{k}(k,h,\varepsilon)$ allow us to guarantee that under the condition $h > 0$ and $h > 0$ there is some value $\varepsilon > 0$ such that $\delta\widetilde{k}(k,h,\varepsilon)=0$. As we have pointed out, δk measures the dispersion of the approximation, as well δk, thus, given h_0 and k_0, a good shape parameter would be $\varepsilon_0(k_0,h_0)$ such that $\delta k(k_0,h_0,\varepsilon_0(k_0,h_0))=0$. Our strategy to reduce numerical dispersion is to find the minimum root of the equation $\delta\widetilde{k}(k_0,h_0,\varepsilon)=0$. For our implementations we will be more restrictive by considering $\frac{1}{4} \le hk \le 1$, with this we are choosing h so that for sampling a wavelength $\lambda=\frac{2\pi}{k}$ it means to use between 2π to 8π points, that is approximately between 6 and 25 points per wavelength. Thus, in our discretization for the Helmholtz equation on hexagonal stencils we will use the shape parameter

$$\varepsilon_{op}(k,h) = \min\{\varepsilon > 0 \;:\; \delta k(k,h,\varepsilon) = 0\}. \tag{51}$$

Figure 5 (Right) shows the results of a test focused on behavior of the optimum shape parameter ε_{op}. A linear dependence of the wavenumber k is observed; at least in the applied test.

ENHANCED LOCAL TRUNCATION ERROR

This section presents the results of a couple of tests intended to show the order of the local truncation error $|\Delta_{H,\varepsilon_{op}}u(x)-\Delta u(x)|$ and $|(\partial_x)_{H,\varepsilon_{op}}u(x)-(\partial_x)u(x)|$. In **Figure 6** shows the results of testing the approximations by comparing with standard FD for $u(x)=e^{ik\cdot x}$. Whereas in **Figure 7** the same is done with $u(x)=\frac{i}{4}H_0^{(1)}(k|x|)$. Both functions are solutions of the Helmholtz equation, it can be noted that in these cases the optimum shape parameter oers an error of the order $\mathcal{O}(h^4)$.

RELATIVE PHASE ERROR - POLLUTION EFFECT

As is well known through the vast literature about numerical solutions of Helmholtz equation, k is a key parameter. For large values of k, the solution u is highly fluctuating. To approximate the Helmholtz equation with an acceptable accuracy, the resolution of the discretization for the domain of interest should be adjusted to the wave number according to the so called rule of thumb [17],

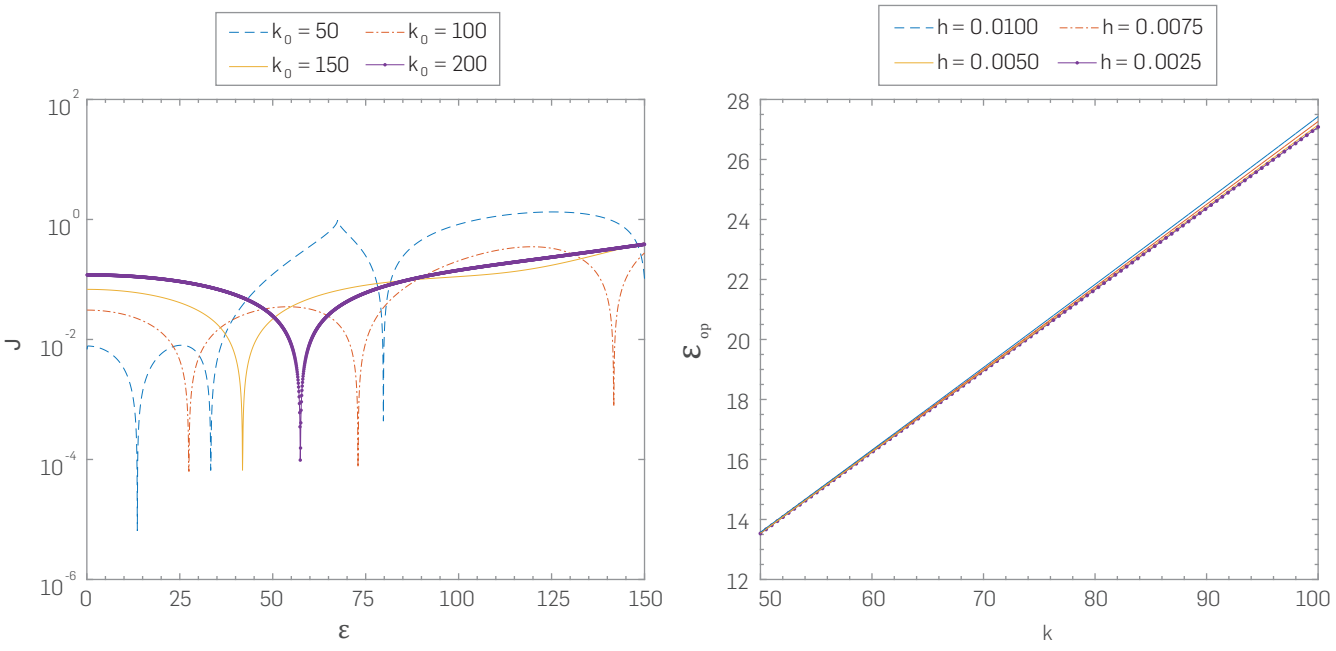

Figure 5 . Left: Plot of $|J(\varepsilon) = \delta k(k_0, \frac{1}{k_0}; \varepsilon)|$ for four different values of k_0. Right: Plot of $\varepsilon = \varepsilon_{op}(100;h)$ for four different values of h.

which prescribes a minimum number of elements per wavelength. However, the performance of standard finite difference or finite element methods, such as the classical Galerkin finite element method, deteriorates as k increases. This misbehavior, known as pollution of the approximate solution, can only be avoided, with standard methods, after a drastic renement of the discretization. [9] summarized the local truncation error $|k^2, h_f^2|/k^2$ and the relative phase error $(k_f,k)|k$ of the most popular methods for solving Helmholtz equation using different size stencils.

Now our aim is to calculate the approximation order of the numerical wavenumber $\widetilde{k}_f$ as k changes, in order to estimate the order of the relative phase error, but first we will examine the order of the error $|\widetilde{k}_f^2 - \widetilde{k}_f^2|$ produced by neglecting the dependence of θ in taking the average value of $\widetilde{k}_f$ on $[0.2\pi]$. We recall that

$$\widetilde{k}_f^2(k,\theta,h,\varepsilon) = 4E(h,\varepsilon) - 2F(h,\varepsilon)T(k,\theta,h) \quad (52)$$

and

$$k_f^2(k,h,\varepsilon) = 4E(h,\varepsilon) - 6F(h,\varepsilon)J_0(hk) \quad (53)$$

From the Taylor polynomials of (44) and Bessel function respectively

$$T(k,\theta,h) = 3 - \frac{3}{4}(hk)^2 + \frac{3}{64}(hk)^4 - \frac{10+\cos(6\theta)}{7680}(hk)^6 + \mathcal{O}(h^8k^8) \quad (54)$$

and

$$3J_0(hk) = 3 - \frac{3}{4}(hk)^2 + \frac{3}{64}(hk)^4 - \frac{1}{768}(hk)^6 + \mathcal{O}(h^8k^8), \quad (55)$$

thus

$$\begin{aligned}\widetilde{k}_f^2 - k_f^2 &= 2F(h,\varepsilon)\left(\frac{\cos(6\theta)}{7680}(hk)^6 + \mathcal{O}(h^8k^8)\right)\\ &= F(h,\varepsilon)\mathcal{O}(h^6k^6).\end{aligned} \quad (56)$$

From the approximations of $F(h,\varepsilon)$ given in (34), it is easy to see that

$$F(h,\varepsilon)\mathcal{O}(h^6k^6) = \mathcal{O}(h^4k^6).$$

Hence $\widetilde{k}_f^2 - \widetilde{k}_f^2 = \mathcal{O}(h^4k^6)$. On the other hand, from (34), (55)

$$\begin{aligned}&\widetilde{k}_f^2(k,\theta,h,\varepsilon)\\ &= 4E(h,\varepsilon) - 6F(h,\varepsilon)\\ &\quad\left(1 - \tfrac{1}{4}(hk)^2 + \tfrac{1}{64}(hk)^4 + \mathcal{O}(h^6k^6)\right)\\ &= 4E(h,\varepsilon) - 6F(h,\varepsilon) + \left(\tfrac{3}{2}h^2F(h,\varepsilon)\right)k^2\\ &\quad - \left(\tfrac{3}{2}h^2F(h,\varepsilon)\right)\tfrac{h^2k^4}{16} + F(h,\varepsilon)\mathcal{O}(h^6k^6)\\ &= k^2 - \tfrac{1}{16}h^2k^4 + \varepsilon^2h^2k^2 - 2\varepsilon^4h^2 + \mathcal{O}(h^4k^6)\\ &\quad + \mathcal{O}(\varepsilon^6h^4) + \mathcal{O}(\varepsilon^2h^4k^4) + \mathcal{O}(\varepsilon^4h^4k^2)\\ &= k^2(1-W),\end{aligned} \quad (57)$$

where

$$\begin{aligned}W = \frac{1}{16}h^2k^2 - \varepsilon^2h^2 + 2\varepsilon^4h^2k^{-2} + \mathcal{O}(h^4k^4)\\ + \mathcal{O}(\varepsilon^6h^4k^{-2}) + \mathcal{O}(\varepsilon^2h^4k^2) + \mathcal{O}(\varepsilon^4h^4).\end{aligned} \quad (58)$$

Provided that $|W| < 1$, the binomial series can be applied, that is $\sqrt{1-W} = 1 - \frac{1}{2}W + \mathcal{O}(W^2)$. We take the linear approximation, then

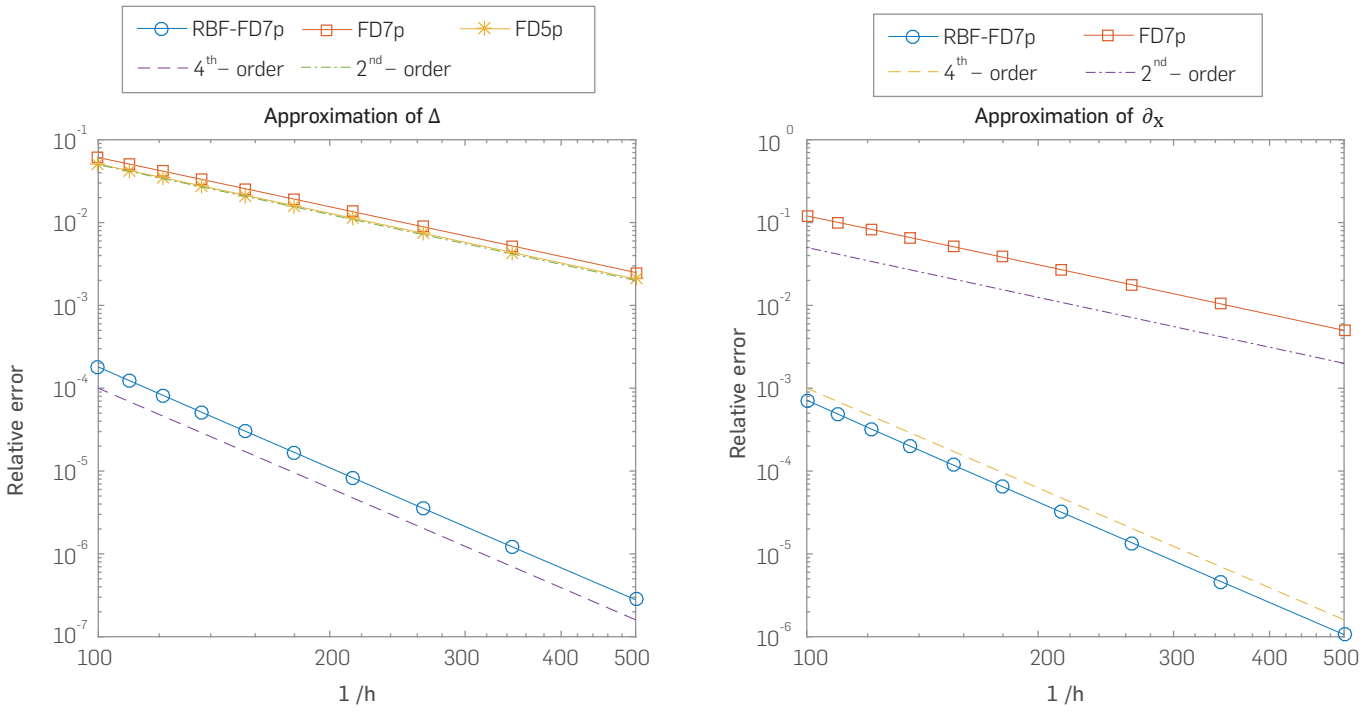

Figure 6 . Left: Comparison of relative local truncation error, varying h, between the approximation using standard FD 7p $\Delta_{H,0}u(x,y)$ and RBF-FD7p $\Delta_{H,0}u(x,y)$. Right: Comparison of relative local truncation error between the approximation using standard FD7p $(\partial_x)_{H,0}u(x,y)$ and RBF-FD7p $(\partial_x)_{H,0}u(x,y)$. Here $u(x,y)=e^{ik(z\cos\theta+y\sin\theta)}$, is evaluated at $(x,y)=(2.15)$, with $\theta=\pi/6$ and k=100.

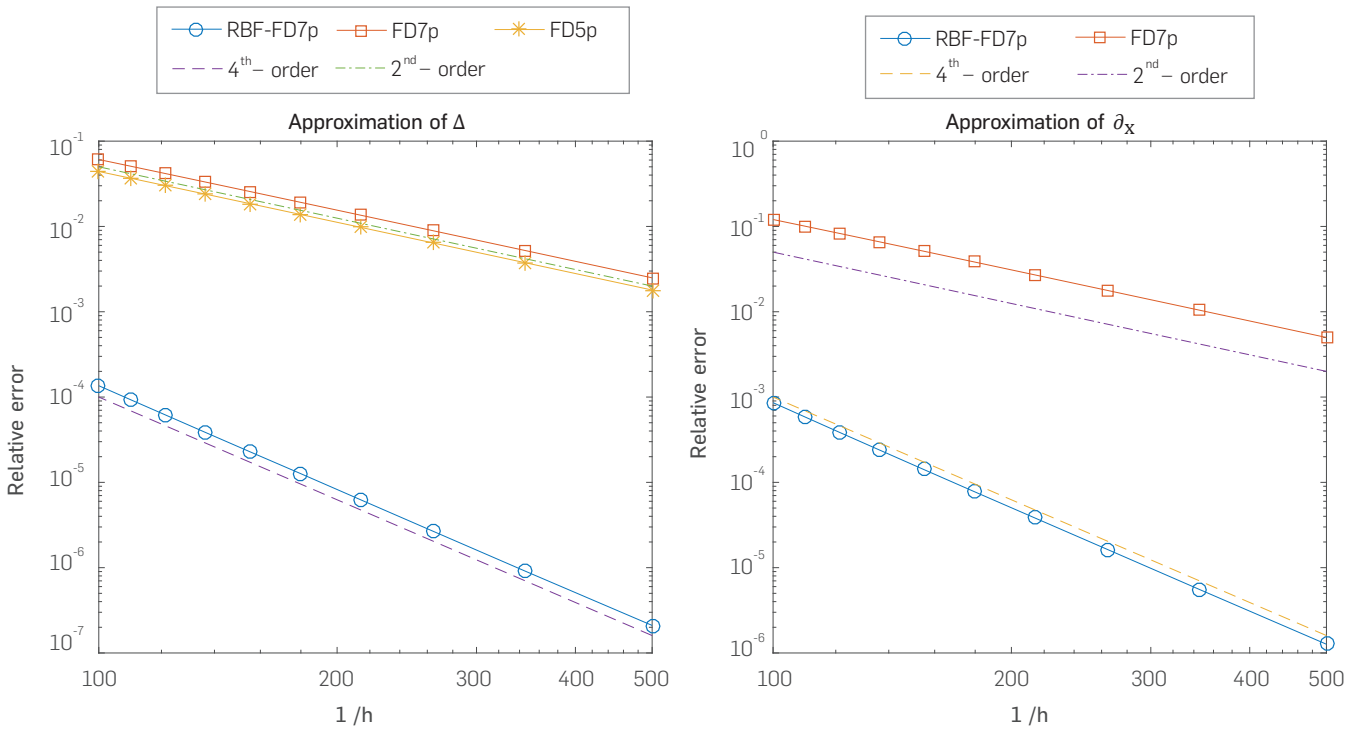

Figure 7 . Left: Comparison of relative local truncation error, varying h, between the approximation using standard FD 7p $\Delta^h u(x,y)$ and RBF-FD7p $(\Delta)_{H,\varepsilon}u(x,y)$. Right: Comparison of relative local truncation error between the approximation using standard FD7p $(\partial_x)^h u(x,y)$ and RBF-FD7p $(\partial_x)_{H,}\varepsilon u(x,y)$. Here $u(x,y)=\frac{i}{4}H_0^{(1)}(k\sqrt{x^2+y^2})$, $H_0^{(1)}$ is the Hankel function evaluated at (x,y) = (2, 1:5) and k = 100.

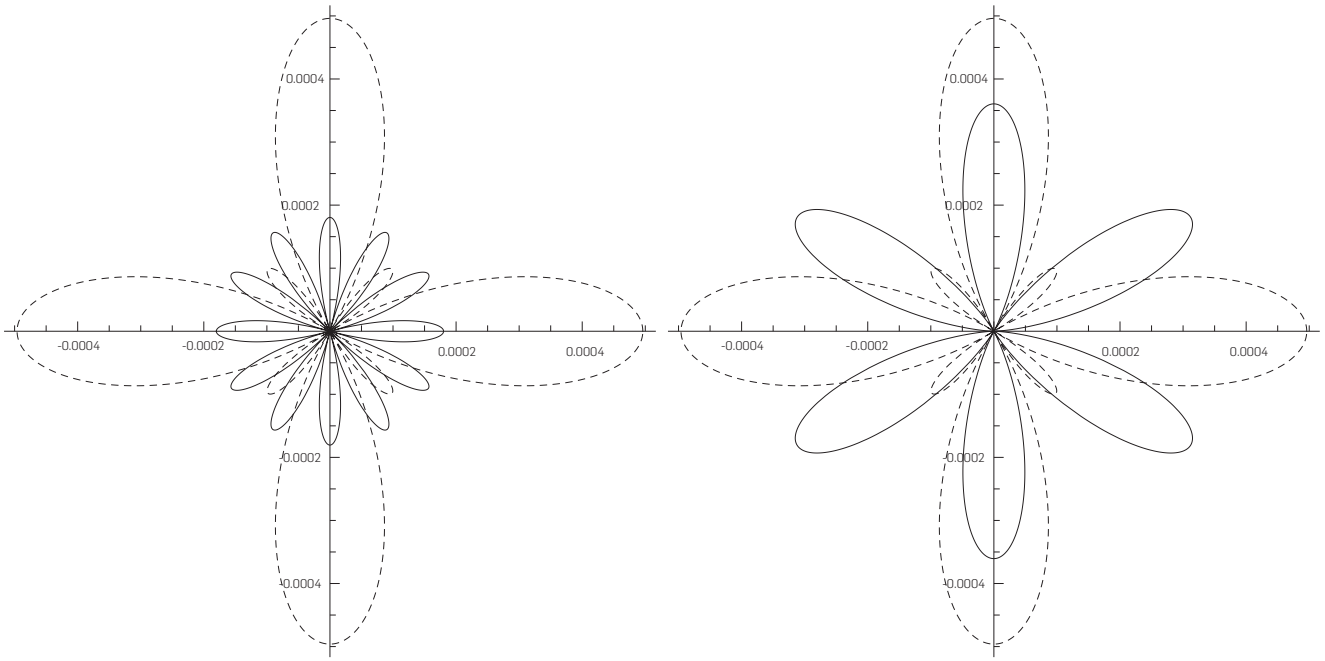

Figure 8 . Comparison between the function $r(\theta)= |\delta\widetilde{k}(k_0,\theta,h_0,\varepsilon_{op})|/k_0^2$(solid line) where $k_0 = 100$ and $h_0 =0.01$, and the function $r(\theta)=J_\gamma(b_0, d_0, e_0;G_0,\theta)/k_0^2$(dashed line) where J_γ and parameters b0, d0, e0 and G0 were taken from [3]. Left: ε_{op} satises $\delta k(100,0.001, \varepsilon_{op})=0$. Right: $\varepsilon_{op}= \arg\min_{\varepsilon>0} |\delta\widetilde{k}(100,\pi/3,0.01,\varepsilon)|$

$$\begin{aligned}\widetilde{k}_f(k,\theta,h,\varepsilon) &= k-\frac{1}{32}h^2k^3+\frac{1}{2}\varepsilon^2h^2k-\varepsilon^4h^2k^{-1}+\mathcal{O}(h^4k^5)\\ &+\mathcal{O}(\varepsilon^6h^4k^{-1})+\mathcal{O}(\varepsilon^2h^4k^3)+\mathcal{O}(\varepsilon^4h^4k).\end{aligned} \tag{59}$$

Hence the relative phase error is given by

$$\begin{aligned}\frac{\widetilde{k}_f-k}{k} &= -\frac{1}{32}h^2k^2+\frac{1}{2}\varepsilon^2h^2-\varepsilon^4h^2k^{-2}+\mathcal{O}(h^4k^4)\\ &+\mathcal{O}(\varepsilon^6h^4k^{-2})+\mathcal{O}(\varepsilon^2h^4k^2)+\mathcal{O}(\varepsilon^4h^4)\end{aligned} \tag{60}$$

Note that for the limit case $\varepsilon \to 0+$

$$\widetilde{k}_f(k,\theta,h,0^+) = k+\mathcal{O}(h^2k^3) \tag{61}$$

which asserts that, in the limit case, for keeping the order of the error when k is increasing, the mesh size h it must scale at least as $k^{-\frac{3}{2}}$, that is $h=\mathcal{O}(k^{-\frac{3}{2}})$.

3. EXPERIMENTAL DEVELOPMENT

Perfectly matched layers (PML) is a technique for simulating solutions of wave phenomena in free-space. The idea is to build an absorbing layer for surrounding the computational domain of interest. The new system possesses the property of generating no reflection, at least in continuous case, at the interface between the free medium and the articial absorbing medium. PML has been introduced by Berenger [1] for Maxwell's equations, and has been widely used for the simulation of time dependent seismic waves as well as Helmholtz-like equations. The analysis necessary to show that the Helmholtz equation with PML (PML-Helmholz) for constant wavenumber is a well-posed problem is treated in [20]. Now a description of PML-Helmholtz equation is given (see [14], [38] for details).

For setting up the PML-Helmholtz equation it is necessary to define some basic functions in a rectangular domain. Let $\sigma_l\ \mathbb{R}\to\mathbb{R}$ be defined by

$$\sigma_l(t)=\begin{cases}0 & \text{for } |t|\le l\\ \frac{\gamma}{\delta}p\left(\frac{|t|-l}{\delta}\right) & \text{for } l<|t|<l+\delta\\ \frac{\gamma}{\delta} & \text{for } |t|\ge l+\delta\end{cases} \tag{62}$$

where $p\ (0,1)\to(0,1)$ is given by $p(t)=1-e^{\frac{t^2}{t^2-1}}$, γ and δ are constant. By definition $\sigma\in C^\infty(\mathbb{R})$. for a fixed positive angular frequency ω satisfying $0<\frac{\gamma}{\delta}<\omega$,let dl be the complex-valued function

$$d_l(t)=1+i\frac{\sigma_l(t)}{\omega} \tag{63}$$

Consider the open rectangles $\Omega=(-a,a)\times(-b,b)$ and $\Omega_\delta=(-a-\delta,a+\delta)\times(-b-\delta,b+\delta)$.

The modified PML-Laplace operator is defined by

$$-\widetilde{\Delta}=-\frac{1}{d_a(x)}\partial_x\left(\frac{1}{d_a(x)}\partial_x\right)-\frac{1}{d_b(y)}\partial_y\left(\frac{1}{d_b(y)}\partial_y\right) \tag{64}$$

or alternatively

$$-\widetilde{\Delta} = -s_a^2(x)\partial_x^2 - s_b^2(y)\partial_y^2 - s_a(x)s_a'(x)\partial_x - s_b(y)s_b'(y)\partial_y \quad (65)$$

where $s_a=\frac{1}{d_a}$ and $s_b=\frac{1}{d_b}$. Note that $-\widetilde{\Delta}$ coincides with $-\Delta$ in Ω. Usually, for making analytic studies this is considered as an unbounded operator on $L^2(\mathbb{R}^2)$ with domain the Sobolev space $H^2(\mathbb{R}^2)$ or in a weaker form, as an unbounded operator on $H^{-1}(\mathbb{R}^2)$ with domain $H^1(\mathbb{R}^2)$ [38]. However, for numerical implementations in the finite difference approach it is considered a truncated version $-\widetilde{\Delta}: C^2(\Omega_\delta)\to C^0(\Omega_\delta)$. The PML-Laplace operator allows to introduce the PML-Helmholtz equation

$$\begin{cases} -\widetilde{\Delta}u - \omega^2 c^{-2}u &= f, \quad \text{in } \Omega_\delta \\ u &= 0, \quad \text{on } \partial\Omega_\delta \end{cases} \quad (66)$$

we will suppose that the function $c = c(x)$ which describe the acoustic or P-wave propagation speed is positive and belongs to $C^2(\Omega_\delta)$.

In order to approximate solutions of equation (66) within the approach of RBF-FD on hexagonal grid, we use the explicit expressions for Gaussian weights, thus by way of the formulas in (33) we have that for x = (x, y) in Ω_δ with 7-stencil $H\subset\Omega_\delta$

$$\begin{aligned}\widetilde{\Delta}_{H,\varepsilon}u(\mathbf{x}) &= s_a^2(x)(\partial_x^2)_{H,\varepsilon}u(\mathbf{x}) + s_b^2(y)(\partial_y^2)_{H,\varepsilon}u(\mathbf{x}) \\ &+ s_a(x)s_a'(x)(\partial_x)_{H,\varepsilon}u(\mathbf{x}) \\ &+ s_b(y)s_b'(y)(\partial_y)_{H,\varepsilon}u(\mathbf{x})\end{aligned} \quad (67)$$

hence by carrying out substitutions

$$\begin{aligned}\widetilde{\Delta}_{H,\varepsilon}u(\mathbf{x}) &= \Gamma_{\mathrm{C}}u_{\mathrm{C}} + \Gamma_{\mathrm{e}}u_{\mathrm{e}} + \Gamma_{\mathrm{w}}u_{\mathrm{w}} + \Gamma_{\mathrm{ne}}u_{\mathrm{ne}} \\ &+ \Gamma_{\mathrm{nw}}u_{\mathrm{nw}} + \Gamma_{\mathrm{se}}u_{\mathrm{se}} + \Gamma_{\mathrm{sw}}u_{\mathrm{sw}}\end{aligned} \quad (68)$$

where weights Γ's are given by

$$\begin{aligned}\Gamma_{\mathrm{C}}(h,\varepsilon,\mathbf{x}) &= -2E(h,\varepsilon)(s_a^2(x)+s_b^2(y)) \\ \Gamma_{\mathrm{e}}(h,\varepsilon,\mathbf{x}) &= F_1(h,\varepsilon)s_a^2(x) + F_2(h,\varepsilon)s_b^2(y) \\ &\quad + 2D(h,\varepsilon)s_a(x)s_a'(x) \\ \Gamma_{\mathrm{w}}(h,\varepsilon,\mathbf{x}) &= F_1(h,\varepsilon)s_a^2(x) + F_2(h,\varepsilon)s_b(y) \\ &\quad - 2D(h,\varepsilon)s_a(x)s_a'(x) \\ \Gamma_{\mathrm{ne}}(h,\varepsilon,\mathbf{x}) &= G_1(h,\varepsilon)s_a^2(x) + G_2(h,\varepsilon)s_b^2(y) \\ &\quad + D(h,\varepsilon)\left(s_a(x)s_a'(x) + \sqrt{3}s_b(y)s_b'(y)\right) \\ \Gamma_{\mathrm{nw}}(h,\varepsilon,\mathbf{x}) &= G_1(h,\varepsilon)s_a^2(x) + G_2(h,\varepsilon)s_b^2(y) \\ &\quad + D(h,\varepsilon)\left(-s_a(x)s_a'(x) + \sqrt{3}s_b(y)s_b'(y)\right) \\ \Gamma_{\mathrm{sw}}(h,\varepsilon,\mathbf{x}) &= G_1(h,\varepsilon)s_a^2(x) + G_2(h,\varepsilon)s_b^2(y) \\ &\quad + D(h,\varepsilon)\left(-s_a(x)s_a'(x) - \sqrt{3}s_b(y)s_b'(y)\right) \\ \Gamma_{\mathrm{se}}(h,\varepsilon,\mathbf{x}) &= G_1(h,\varepsilon)s_a^2(x) + G_2(h,\varepsilon)s_b^2(y) \\ &\quad + D(h,\varepsilon)\left(s_a(x)s_a'(x) - \sqrt{3}s_b(y)s_b'(y)\right)\end{aligned} \quad (69)$$

and of course,

$$\begin{aligned}&\widetilde{\Delta}_{H,\varepsilon}u(\mathbf{x}) + \omega^2 c^{-2}(\mathbf{x})u(\mathbf{x}) \\ &= (\Gamma_{\mathrm{C}} + \omega^2 c^{-2}(\mathbf{x}))u_{\mathrm{C}} + \Gamma_{\mathrm{e}}u_{\mathrm{e}} + \Gamma_{\mathrm{w}}u_{\mathrm{w}} \\ &+ \Gamma_{\mathrm{ne}}u_{\mathrm{ne}} + \Gamma_{\mathrm{nw}}u_{\mathrm{nw}} + \Gamma_{\mathrm{se}}u_{\mathrm{se}} + \Gamma_{\mathrm{sw}}u_{\mathrm{sw}}\end{aligned} \quad (70)$$

We use the optimal shape parameter ε given by (51) to approximate each operator involved in (68). To analyze the approximation $\widetilde{\Delta}_{H,\varepsilon}u(x)$ applied to problem (66) we regard the concept of consistency [32].

Definition 2. Given a partial differential equation, $\mathcal{L}u = f$, and a finite difference scheme, $\mathcal{L}_h u = f$ based on a stencil with size h, we say that the finite difference scheme is consistent with the partial differential equation if for any smooth function φ(x)

$$\mathcal{L}\varphi - \mathcal{L}_h\varphi \to 0 \quad (71)$$

as $h \to 0$, the convergence being pointwise convergence at each point x.

Proposition 1. The RBF-FD approximation given in (67) applied to the problem (66) is consistent with the Helmholtz-PML equation and has second order of accuracy.

Proof. We need to show that for an hexagonal 7−stencil H of size h centered at $x\in\Omega_\delta$ and for a given shape parameter ε

$$\begin{aligned}&\left(-\widetilde{\Delta} - \omega^2 c(\mathbf{x})^{-2}\right)\varphi(\mathbf{x}) - \left(-\widetilde{\Delta}_{H,\varepsilon} - \omega^2 c(\mathbf{x})^{-2}\right)\varphi(\mathbf{x}) \\ &= \widetilde{\Delta}_{H,\varepsilon}\varphi(\mathbf{x}) - \widetilde{\Delta}\varphi(\mathbf{x})\end{aligned} \quad (72)$$

converges pointwise to 0 as $h \to 0$, where φ is a smooth function. The proof will be completed by simply inspecting the estimates in (38) used in (67), once performed these substitutions we can observe that

$$|\widetilde{\Delta}_{H,\varepsilon}\varphi(\mathbf{x}) - \widetilde{\Delta}\varphi(\mathbf{x})| = \mathcal{O}(\varepsilon^2 h^2), \quad (73)$$

which means that the accuracy of the approximation is $\mathcal{O}(\varepsilon^2 h^2)$, as εh tends to 0.

DISCRETE FORMULATION

We will perform the discretization of the problem (66) on an hexagonal grid G which represents to Ω_δ. The optimal shape parameter at every stencil will be taken in accord to its dependence of the local wavenumber $k(x) = \omega^2 c^{-2}(x)$, so $\varepsilon_{op}(x) = \varepsilon_{op}(k(x),h)$, where is used (51). For the sake of a more simplied notation, we denote similarly for the others weights formulas in (69).

$$\Gamma_{\mathrm{C}}(\mathbf{x}) = \Gamma_{\mathrm{C}}(h, \varepsilon_{op}(\mathbf{x}), \mathbf{x}), \quad (74)$$

We begin by considering two rectangular grids given by

$$\begin{aligned}G^1 &= \left\{\left(mh, n\sqrt{3}h\right) \ : \ m = 0,\ldots, N_x - 1;\ n = 0,\ldots,\tfrac{N_z-1}{2}\right\} \\ G^2 &= \left\{\left(\left(m-\tfrac{1}{2}\right)h, \left(n+\tfrac{1}{2}\right)\sqrt{3}h\right) \right. \\ &\quad \left. : \ m = 0,\ldots,N_x;\ n = 0,\ldots,\tfrac{N_z-3}{2}\right\}\end{aligned} \quad (75)$$

where N_z is a positive odd integer. Note that the grid $G = G^1\cup G^2$ is formed by hexagonal stencils. We denote $x^1_{mn} = (mh, n\sqrt{3}h)$ and $x^2_{mn} = ((m-\frac{1}{2})h, (n+\frac{1}{2})\sqrt{3}h)$ for points in G^1 and G^2 respectively; also we denote $u^j_{mn} = u(x^j_{mn})$ for $x^j_{mn}\in G^j$, $j = 1, 2$. The homogeneous Dirichlet boundary condition it is expressed in terms of the boundary points of the grid G, by doing

$$\begin{aligned}&u^1_{m,0} = u^1_{m,\frac{Nz-1}{2}} = u^1_{N_x-1,n} = u^1_{0,n} \\ &= 0; \text{ for } m = 0,\ldots,N_x-1;\ n = 0,\ldots,\frac{N_z-1}{2}\end{aligned} \quad (76)$$

$$u^2_{0,n} = u^2_{N_x,n} = 0; \text{ for } n = 0, \ldots, \frac{N_z - 3}{2} \tag{77}$$

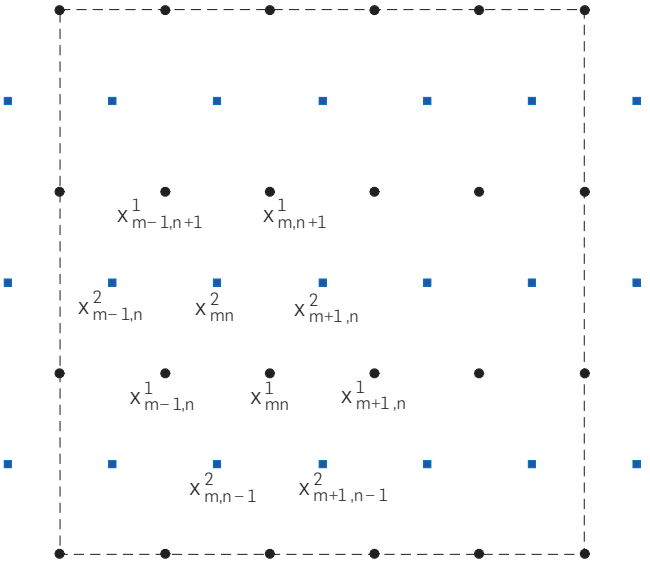

Figure 9 . Hexagonal grid $G = G^1 \cup G^2$, where G^1 are black dots and G^2 are blue squares.

Thus, for points in the grid G1, the equation (68) has the explicit form

$$\begin{aligned}&\Gamma_{\mathrm{sw}} u^2_{m,n-1} + \Gamma_{\mathrm{se}} u^2_{m+1,n-1} + \Gamma_{\mathrm{w}} u^1_{m-1,n} \\ &+ \Gamma_{\mathrm{c}} u^1_{m,n} + \Gamma_{\mathrm{e}} u^1_{m+1,n} + \Gamma_{\mathrm{nw}} u^2_{m,n} + \Gamma_{\mathrm{ne}} u^2_{m+1,n} \\ &= -f(\mathbf{x}^1_{mn})\end{aligned} \tag{78}$$

for $m = 1,\ldots,N_x - 2$, $n = 1, \ldots, \frac{N_z-3}{2}$, and for points at grid G^2 is

$$\begin{aligned}&\Gamma_{\mathrm{sw}} u^1_{m-1,n} + \Gamma_{\mathrm{se}} u^1_{m,n} + \Gamma_{\mathrm{w}} u^2_{m-1,n} + \Gamma_{\mathrm{c}} u^2_{m,n} \\ &+ \Gamma_{\mathrm{e}} u^2_{m+1,n} + \Gamma_{\mathrm{nw}} u^2_{m-1,n+1} + \Gamma_{\mathrm{ne}} u^1_{m,n+1} = -f(\mathbf{x}^2_{mn})\end{aligned} \tag{79}$$

for $m = 1,\ldots,N_x - 1$, $n = 0, \ldots, \frac{N_z-3}{2}$. With the couple of equations above we assemble a sparse linear system $(-\widetilde{\Delta}_h - \omega^2 c^{-2})U_h = f$ where c is a diagonal matrix formed with the values $c^j_{mn} = c(x^j_{mn})$,

$$\widetilde{\Delta}_h = \begin{pmatrix} \mathbf{C}^2_0 & \mathbf{N}^1_1 & \mathbf{0} & \mathbf{0} & \cdots & \mathbf{0} & \mathbf{0} & \mathbf{0} \\ \mathbf{S}^2_0 & \mathbf{C}^1_1 & \mathbf{N}^2_1 & \mathbf{0} & \cdots & \mathbf{0} & \mathbf{0} & \mathbf{0} \\ \mathbf{0} & \mathbf{S}^1_1 & \mathbf{C}^1_2 & \mathbf{N}^1_2 & & \mathbf{0} & \mathbf{0} & \mathbf{0} \\ \mathbf{0} & \mathbf{0} & \mathbf{S}^2_1 & \mathbf{C}^1_2 & & \mathbf{0} & \mathbf{0} & \mathbf{0} \\ \vdots & \vdots & & & \ddots & & & \vdots \\ \mathbf{0} & \mathbf{0} & \mathbf{0} & \mathbf{0} & & \mathbf{C}^2_{\frac{N_z-5}{2}} & \mathbf{N}^1_{\frac{N_z-3}{2}} & \mathbf{0} \\ \mathbf{0} & \mathbf{0} & \mathbf{0} & \mathbf{0} & & \mathbf{S}^2_{\frac{N_z-5}{2}} & \mathbf{C}^1_{\frac{N_z-3}{2}} & \mathbf{N}^2_{\frac{N_z-3}{2}} \\ \mathbf{0} & \mathbf{0} & \mathbf{0} & \mathbf{0} & \cdots & \mathbf{0} & \mathbf{S}^1_{\frac{N_z-3}{2}} & \mathbf{C}^2_{\frac{N_z-3}{2}} \end{pmatrix} \tag{80}$$

is a block matrix whose blocks are given by

$$\mathbf{C}^1_n = \begin{pmatrix} \Gamma_{\mathrm{c}}(\mathbf{x}^1_{1,n}) & \Gamma_{\mathrm{e}}(\mathbf{x}^1_{2,n}) & 0 & \cdots & 0 & 0 \\ \Gamma_{\mathrm{w}}(\mathbf{x}^1_{1,n}) & \Gamma_{\mathrm{c}}(\mathbf{x}^1_{2,n}) & \Gamma_{\mathrm{e}}(\mathbf{x}^1_{3,n}) & & 0 & 0 \\ 0 & \Gamma_{\mathrm{w}}(\mathbf{x}^1_{2,n}) & \Gamma_{\mathrm{c}}(\mathbf{x}^1_{3,n}) & & 0 & 0 \\ \vdots & & & \ddots & & \\ 0 & 0 & 0 & & \Gamma_{\mathrm{c}}(\mathbf{x}^1_{N_x-3,n}) & \Gamma_{\mathrm{e}}(\mathbf{x}^1_{N_x-2,n}) \\ 0 & 0 & 0 & & \Gamma_{\mathrm{w}}(\mathbf{x}^1_{N\ \ 3}) & \Gamma_{\mathrm{c}}(\mathbf{x}^1_{N\ \ 2}) \end{pmatrix} \tag{81}$$

$$\mathbf{C}^2_n = \begin{pmatrix} \Gamma_{\mathrm{c}}(\mathbf{x}^2_{1,n}) & \Gamma_{\mathrm{e}}(\mathbf{x}^2_{2,n}) & 0 & \cdots & {}^{x-,n}0 & {}^{x-,n}0 \\ \Gamma_{\mathrm{w}}(\mathbf{x}^2_{1,n}) & \Gamma_{\mathrm{c}}(\mathbf{x}^2_{2,n}) & \Gamma_{\mathrm{e}}(\mathbf{x}^2_{3,n}) & & 0 & 0 \\ 0 & \Gamma_{\mathrm{w}}(\mathbf{x}^2_{2,n}) & \Gamma_{\mathrm{c}}(\mathbf{x}^2_{3,n}) & & 0 & 0 \\ \vdots & & & \ddots & & \\ 0 & 0 & 0 & & \Gamma_{\mathrm{c}}(\mathbf{x}^2_{N_x-2,n}) & \Gamma_{\mathrm{e}}(\mathbf{x}^2_{N_x-1,n}) \\ 0 & 0 & 0 & & \Gamma_{\mathrm{w}}(\mathbf{x}^2_{N_x-2,n}) & \Gamma_{\mathrm{c}}(\mathbf{x}^2_{N_x-1,n}) \end{pmatrix} \tag{82}$$

$$\mathbf{N}^1_n = \begin{pmatrix} \Gamma_{\mathrm{ne}}(\mathbf{x}^1_{1,n}) & 0 & \cdots & 0 & 0 \\ \Gamma_{\mathrm{nw}}(\mathbf{x}^1_{1,n}) & \Gamma_{\mathrm{ne}}(\mathbf{x}^1_{2,n}) & & 0 & 0 \\ 0 & \Gamma_{\mathrm{nw}}(\mathbf{x}^1_{2,n}) & & 0 & 0 \\ \vdots & & \ddots & & \\ 0 & 0 & & \Gamma_{\mathrm{nw}}(\mathbf{x}^1_{N_x-3,n}) & \Gamma_{\mathrm{ne}}(\mathbf{x}^1_{N_x-2,n}) \\ 0 & 0 & \cdots & 0 & \Gamma_{\mathrm{nw}}(\mathbf{x}^1_{N_x-2,n}) \end{pmatrix} \tag{83}$$

$$\mathbf{N}_n^2 = \begin{pmatrix} \Gamma_{\mathrm{nw}}(\mathbf{x}_{1,n}^2) & \Gamma_{\mathrm{ne}}(\mathbf{x}_{2,n}^2) & 0 & \cdots & 0 & 0 \\ 0 & \Gamma_{\mathrm{nw}}(\mathbf{x}_{2,n}^2) & \Gamma_{\mathrm{ne}}(\mathbf{x}_{3,n}^2) & & 0 & 0 \\ \vdots & & & \ddots & & \vdots \\ 0 & 0 & 0 & & \Gamma_{\mathrm{ne}}(\mathbf{x}_{N_x-2,n}^2) & 0 \\ 0 & 0 & 0 & & \Gamma_{\mathrm{nw}}(\mathbf{x}_{N_x-2,n}^2) & \Gamma_{\mathrm{ne}}(\mathbf{x}_{N_x-1,n}^2) \end{pmatrix} \tag{84}$$

$$\mathbf{S}_n^1 = \begin{pmatrix} \Gamma_{\mathrm{se}}(\mathbf{x}_{1,n}^1) & 0 & \cdots & 0 & 0 \\ \Gamma_{\mathrm{sw}}(\mathbf{x}_{1,n}^1) & \Gamma_{\mathrm{se}}(\mathbf{x}_{2,n}^1) & & 0 & 0 \\ 0 & \Gamma_{\mathrm{sw}}(\mathbf{x}_{2,n}^1) & & 0 & 0 \\ \vdots & & \ddots & & \\ 0 & 0 & & \Gamma_{\mathrm{sw}}(\mathbf{x}_{N_x-3,n}^1) & \Gamma_{\mathrm{se}}(\mathbf{x}_{N_x-2,n}^1) \\ 0 & 0 & \cdots & 0 & \Gamma_{\mathrm{sw}}(\mathbf{x}_{N_x-2\,n}^1) \end{pmatrix} \tag{85}$$

$$\mathbf{S}_n^2 = \begin{pmatrix} \Gamma_{\mathrm{sw}}(\mathbf{x}_{1,n}^2) & \Gamma_{\mathrm{se}}(\mathbf{x}_{2,n}^2) & 0 & \cdots & 0 & 0 \\ 0 & \Gamma_{\mathrm{sw}}(\mathbf{x}_{2,n}^2) & \Gamma_{\mathrm{se}}(\mathbf{x}_{3,n}^2) & & 0 & 0 \\ \vdots & & & \ddots & & \vdots \\ 0 & 0 & 0 & & \Gamma_{\mathrm{se}}(\mathbf{x}_{N_x-2,n}^2) & 0 \\ 0 & 0 & 0 & & \Gamma_{\mathrm{sw}}(\mathbf{x}_{N_x-2,n}^2) & \Gamma_{\mathrm{se}}(\mathbf{x}_{N_x-1,n}^2) \end{pmatrix} \tag{86}$$

$$\mathbf{U}_h = \left(u_{1,1}^2 \cdots u_{N_x-1,1}^2 \; u_{1,1}^1 \cdots u_{N_x-2,1}^1 \;\; u_{1,2}^2 \cdots u_{Nx-1,2}^2 \cdots u_{1,\frac{N_z-5}{2}}^1 \cdots \right. \tag{87}$$

$$\left. u_{N_x-2,\frac{N_z-5}{2}}^1 \; u_{1,\frac{N_z-3}{2}}^2 \cdots u_{Nx-1,\frac{N_z-3}{2}}^2 \right) \tag{88}$$

$$\mathbf{f} = \left(f_{1,1}^2 \cdots f_{N_x-1,1}^2 \; f_{1,1}^1 \cdots f_{N_x-2,1}^1 \;\; f_{1,2}^2 \cdots f_{Nx-1,2}^2 \cdots f_{1,\frac{N_z-5}{2}}^1 \cdots \right. \tag{89}$$

$$\left. f_{N_x-2,\frac{N_z-5}{2}}^1 \; f_{1,\frac{N_z-3}{2}}^2 \cdots f_{Nx-1,\frac{N_z-3}{2}}^2 \right) \tag{90}$$

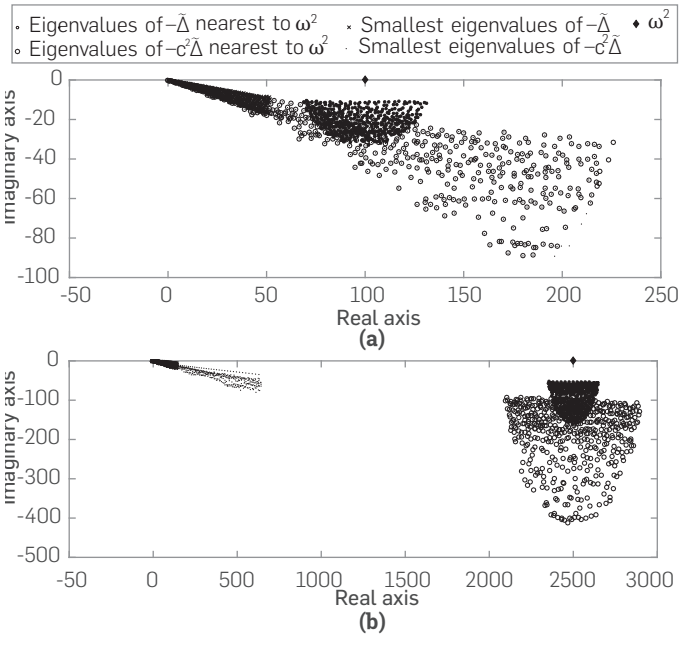

Figure 10. Plot of some eigenvalues of the matrices $-\tilde{\Delta}_h$ and $-c^2\tilde{\Delta}_h$ (Top) for $\omega = 10$ and $h = 0.1497$, (below) $\omega = 50$ and $h = 0.0300$. c represents the Marmousi model extended to PML.

The sparsity pattern of the matrix $\tilde{\Delta}_h$ is depicted in **Figure 11**.

Remark 3. *If* $L_h = (-\tilde{\Delta}_h - \omega^2 c^{-2})$, the linear system $L_h U_h = \mathbf{f}$ can be solved if only if $\omega^2 \notin \sum(-c^2\tilde{\Delta}_h)$. Here $\sum(A)$ denotes the spectrum of A. Is pending for a further work to prove that $\omega^2 \notin \sum(-c^2\tilde{\Delta}_h)$. **Figure 10** shows a plot of some eigenvalues of the matrices $-\tilde{\Delta}_h$ and $-c^2\tilde{\Delta}_h$, where c represents the Marmousi model extended to PML. The eigenvalues plotted are 500 nearest to ω^2 and 500 nearest to 0.

4. RESULTS

EXACT IMPEDANCE BOUNDARY CONDITIONS

$$\begin{aligned} -\Delta u - k^2 u &= f, \text{ in } \Omega \\ ik\mathcal{B}u + \frac{\partial u}{\partial n} &= g, \text{ on } \partial\Omega \end{aligned} \tag{91}$$

PLANE WAVES

With $\Omega = (0,1) \times (0,1)$, $k = 500$, $k_x = k \cos\theta$, $k_z = k \sin\theta$. By using 2π points per wavelength, *i.e.* $kh = 1$, we solve (91)

with g given by $g(x, z)$

$$= \begin{cases} i(k - k_z)e^{ik_x x}, & \text{if } z = 0 \\ i(k + k_x)e^{i(k_x + k_z z)} & \text{if } x = 1 \\ i(k + k_z)e^{i(k_x x + k_z)} & \text{if } z = 1 \\ i(k - k_x)e^{ik_z z} & \text{if } x = 0 \end{cases}$$

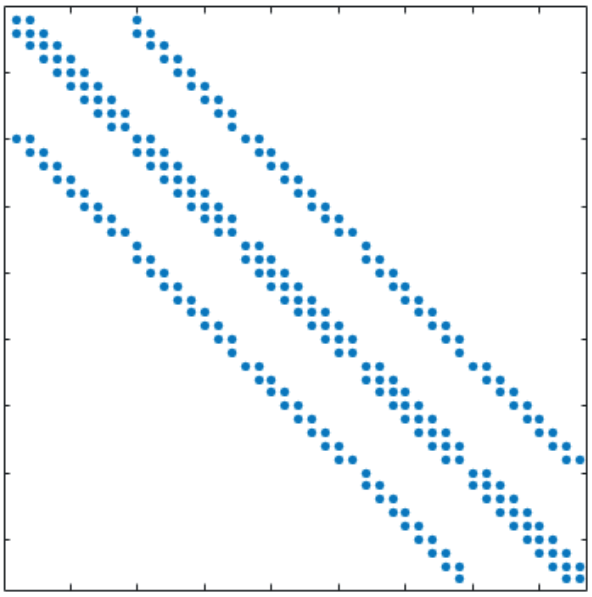

Figure 11. Sparsity pattern of the matrix $\widetilde{\Delta}_h$

The results can be seen in Figure13.

SPHERICAL WAVEFRONT

For this example it is chosen $N_g = 6$ for solving the problem (91) with $\Omega = (0, 1)\times(0, 1)$. Where g is the boundary data satisfying the exact solutions

$$u_1(x,y) = H_0^{(1)}(k\sqrt{(x-2)^2+(y-2)^2}), \tag{92}$$

and

$$\begin{aligned} u_2(x,y) &= \sqrt{k}H_0^{(1)}(k\sqrt{(x+20)^2+(y+20)^2}) \\ &+ 2\sqrt{k}H_0^{(1)}(k\sqrt{(x-20)^2+(y-20)^2}) \\ &+ 0.5\sqrt{k}H_0^{(1)}(k\sqrt{(x+20)^2+(y-20)^2}) \\ &- \sqrt{k}H_0^{(1)}(k\sqrt{(x-20)^2+(y+20)^2}), \end{aligned} \tag{93}$$

with constant k. These solutions corresponds to a single source and four sources, respectively, outside the domain Ω. The relevancy of taking u_2 can be seen in [13]. Discretizations were made with N_g = 6 nodes per wavelength at each value of the wavenumber k. Within an hexagonal grid we take 7–stencils at inner nodes and 22–stencils at boundary nodes.

Table 1. Error of the approximated solutions $\widetilde{u}_1$ and $\widetilde{u}_2$ for the problem (91) with source outside the domain, whose exact solution u_1 and u_2 are given in (92) and (93).

k	50	100	200	400	800
2π–h	30	600	1200	2400	4200
N	2691	10604	42214	168847	674614
N_{nh}	608	1379	3441	5460	10106
N_b	206	412	822	1646	3290
$\|\|u_c-\widetilde{u}_c\|\|_{L^2}$	1.28e-03	9.84e-04	8.15e-04	6.11e-04	6.11e-04
$\|\|u_c-\widetilde{u}_c\|\|_{L^2}/\|\|u_c\|\|_{L^2}$	1.78e-02	1.91e-02	2.24e-02	2.38e-02	3.36e-02
$\|\|u_c-\widetilde{u}_c\|\|_{L^2}$	7.27e-03	7.15e-03	7.41e-03	6.07e-03	6.40e-03
$\|\|u_c-\widetilde{u}_c\|\|_{L^2}/\|\|u_c\|\|_{L^2}$	2.09e-02	2.04e-02	2.11e-02	1.73e-02	1.82e-02

INSIDE SOURCE PROBLEM

Now we test our method with sources inside the domain. The aim is to get the truncated solution of the problem

$$u_c(x,y) = \frac{i}{4}H_0^{(1)}(k\sqrt{(x-0.5)^2+(y-0.5)^2}), \tag{94}$$

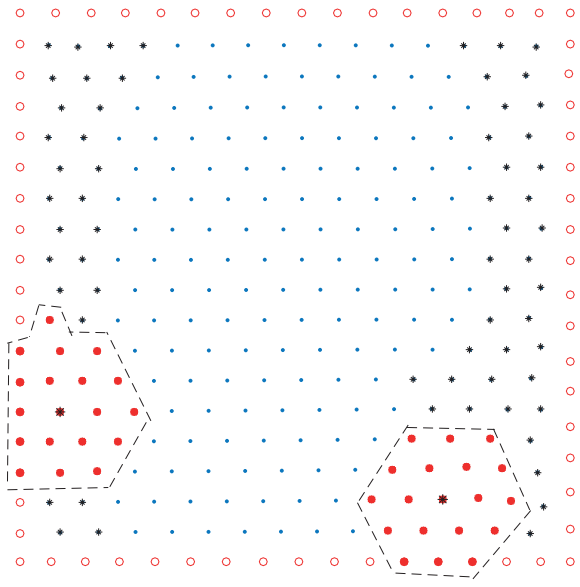

Figure 12. Nodes distribution of hexagonal type.

$$\begin{aligned} u_M(x,y) &= \frac{i}{4}H_0^{(1)}(k\sqrt{(x-0.5)^2+(y-0.5)^2}) \\ &+ \frac{i}{4}H_0^{(1)}(k\sqrt{(x-0.25)^2+(y-0.25)^2}), \end{aligned} \tag{95}$$

Table 2. Error of the approximated solutions $\widetilde{u}_1$ and $\widetilde{u}_2$ for the problem (91) with source f inside the domain, $g = 0$ and $\mathcal{B}$ the third order Pade approximation. Exact solutions u_c and u_M are given in (94) and (95).

k	50	100	200	400	800
2π–h	30	600	1200	2400	4200
N	2691	10604	42214	168847	674614
N_{nh}	608	1379	3441	5460	10106
N_b	206	412	822	1646	3290
$\|\|u_c-\widetilde{u}_c\|\|_{L^2}$	3.13e-03	1.69e-03	1.97e-03	1.27e-03	8.70e-04
$\|\|u_c-\widetilde{u}_c\|\|_{L^2}/\|\|u_c\|\|_{L^2}$	6.45e-02	4.91e-02	8.00e-02	7.28e-02	7.03e-02
$\|\|u_M-\widetilde{u}_M\|\|_{L^2}$	4.15e-03	2.72e-03	2.38e-03	1.73e-03	1.27e-03
$\|\|u_M-\widetilde{u}_M\|\|_{L^2}/\|\|u_M\|\|_{L^2}$	6.54e-02	6.10e-02	6.83e-02	7.39e-02	7.34e-02

WITH PML

In this test we solve the problem of nd the truncated Green's function for $-\widetilde{\Delta}_h - k^2$ in $\Omega = (0, 1) \times (0, 1)$, that is the solution of

$$\begin{aligned} (-\widetilde{\Delta} - k^2)u(x,z) &= \widetilde{\delta}(x-0.25, z-5\times10^{-4}) \\ &+ \widetilde{\delta}(x-0.5, z-5\times10^{-4}) + \widetilde{\delta}(x-0.75, z-5\times10^{-4}). \end{aligned}$$

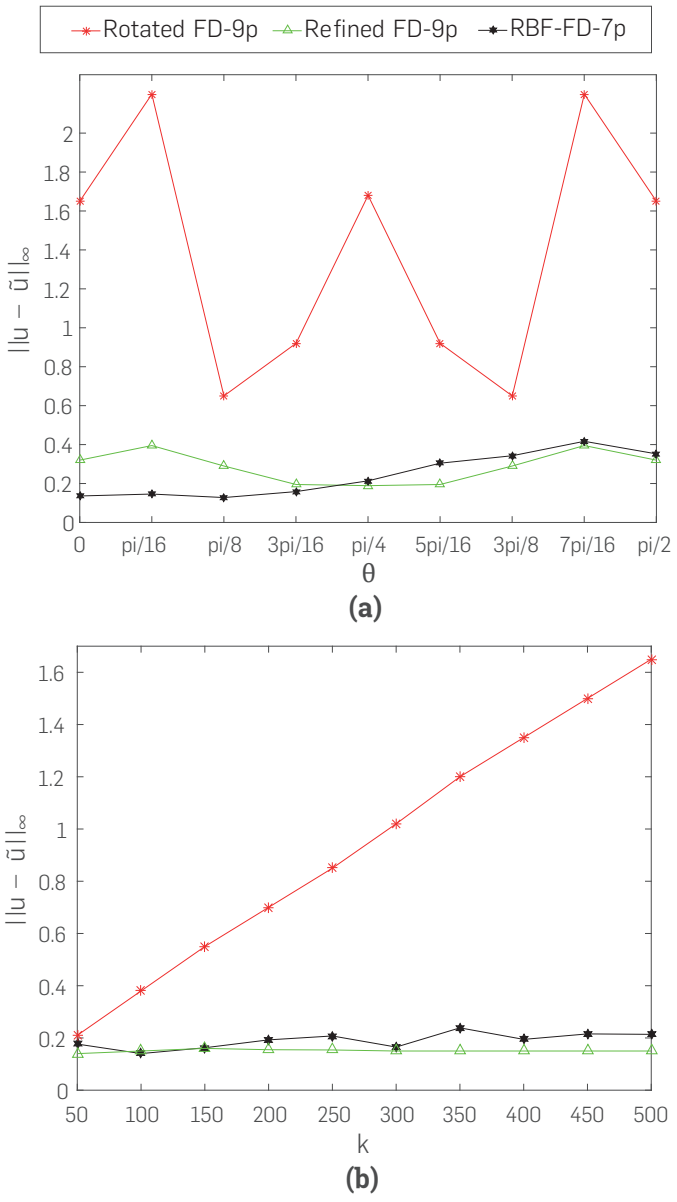

Figure 13. Comparison of results between RBF-FD and those reported in [3]. (a) Results for k = 500 and h = 1/500 varying the propagation angle. (b) With k varying, $\theta=\pi/4$ and $h=1/k$

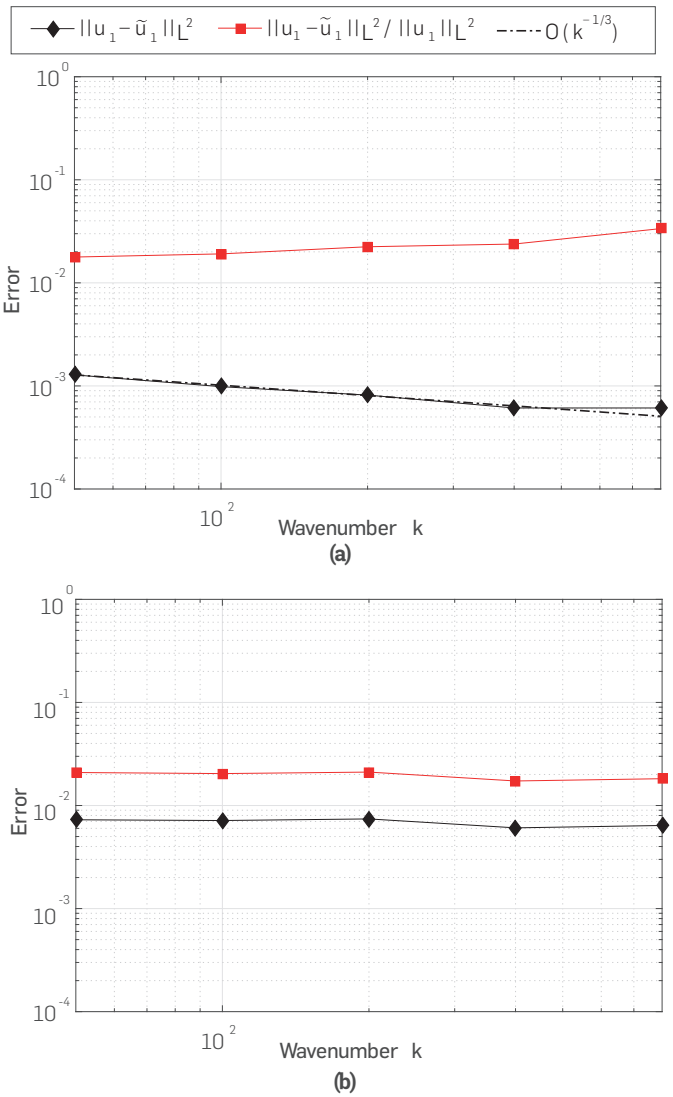

Figure 14. Plot of tests for approximated solutions of (91). (a) Comparison with the exact solution (92). (b) Comparison with the exact solution (93).

The solution of this problem is

$$
\begin{aligned}
u(x,y) &= H_0^{(1)}(k\sqrt{(x-0.25)^2+(z-5\times10^{-4})^2}) \\
&+ H_0^{(1)}(k\sqrt{(x-0.5)^2+(z-5\times10^{-4})^2}) \\
&+ H_0^{(1)}(k\sqrt{(x-0.75)^2+(z-5\times10^{-4})^2})
\end{aligned} \tag{96}
$$

where $H_0^{(1)}$ is the Hankel function. For this test we use 2π points per wavelength (*i.e.* $kh = 1$). Some results with a qualitative analysis of error are shown in **Figure 15**.

2004 BP MODEL

In this example we calculate the truncated Green function for the well known BP model in frequencies 15Hz and 40Hz. The results are shown in **Figure 16**.

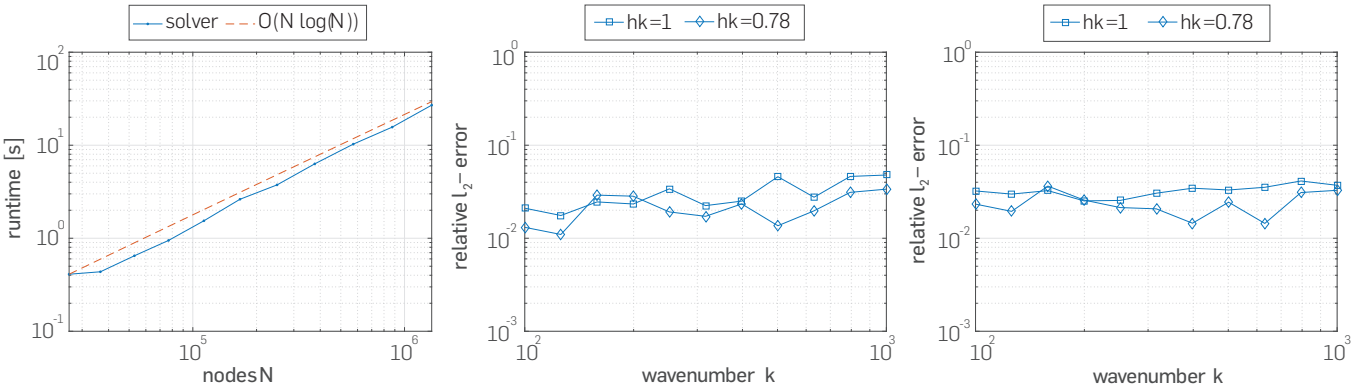

Figure 15. (Left) Runtime for solving the system $L_h U_h = f$ by LU factorization. (Center) Near boundary sources. (Right) Centered sources.

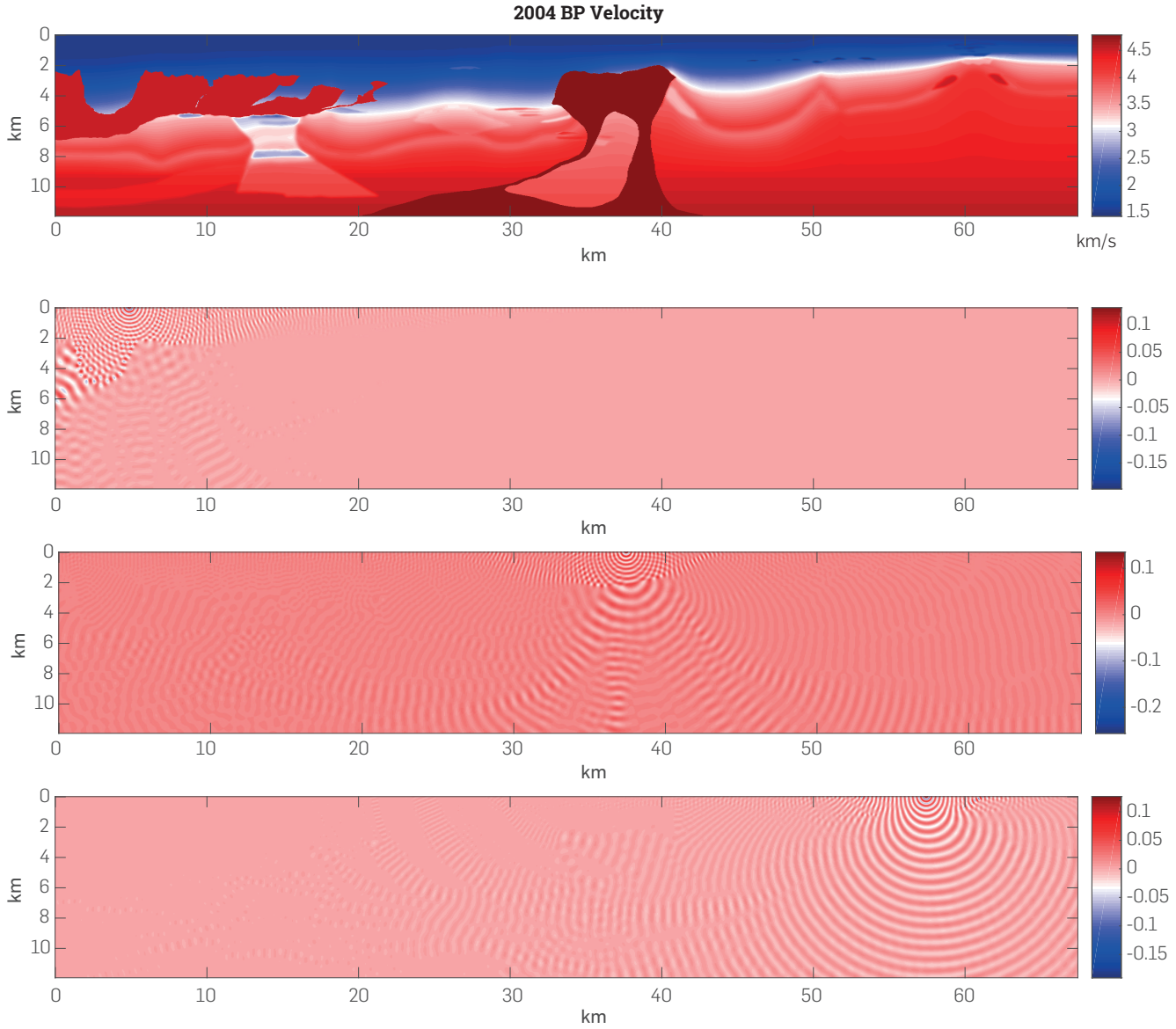

Figure 16. Top: 2004 BP velocity-analysis Benchmark. Bottom plots: Real part of the wave eld at 6Hz with dierent positions of the source.

CONCLUSIONS

In this paper we have developed and applied a RBF-FD method on hexagonal grids that solves the Helmholtz equation for a wide range of values of the wavenumber k. We focus in obtaining accurate local approximations of the partial derivative operators by using a few degrees of freedom applied to solutions of Helmholtz equation.

We obtain closed formulas for the weights in terms of ε, h showing that the standard finite difference method is the limit of our RBF-FD scheme, this happens when the wide of the Gaussian RBF, controlled by the shape parameter ε, tends to be flat. The method obtains banded matrices; such that the respective linear systems can be solved efficiently by direct solvers.

We have developed a simple solver that is compared with 5-point Finite difference method and accurate compared with 9-point FD method. By local interpolation we found good shape parameters to approximate derivatives of solutions of the 2D Helmholtz equation. Within the RBF-FD framework are approximated the solutions of the PMLHelmholtz equation on hexagonal grids with optimal values of the shape parameter.

Our method has been compared against classical and well-known methods, showing equal and sometimes better performance. with this we have validated numerically that our solver suer less of the pollution effects. The advantages and drawbacks of the RBF-FD method applied to Helmholtz equation can be seen at Table 3.

Table 3. Advantages and drawbacks of RBF-FD method

Strength	Drawbacks
It doesn't require a mesh. Rather than discretizing space, the solutions are approximated by a set of basis functions. The method only needs to use collocation points in the domain and on the border	The resulting linear equation system may have a bad conditioning. This problem has been treated with different matrix conditioning methods
Simpler numerical implementation and lower computational cost	Lower quality approach near the border.
You can easily increase the support domain, change basis, adopt nodal densities or local refinement.	It requires tuning parameters. Strongly depends on the proper value of shape parameter, whose optimal value is not known a priori
Easily adaptable to irregular domains or higher dimensions.	It is difficult to find formulas for error bounds in interpolation
It is efficient in terms of computational time and can be readily parallelized	If the number of nodes changes, it is necessary to change the shape parameter accordingly

ACKNOWLEDGEMENTS

This work is supported by Colombian Oil Company ECOPETROL and COLCIENCIAS as a part of the research project grant No. 0266-2013.

REFERENCES

[1] Jean-Pierre Berenger. A perfectly matched layer for the absorption of electromagnetic waves. Journal of Computational Physics, 114(2):185-200, 1994.

[2] Ivo M. Babuska and Stefan A. Sauter. Is the pollution effect of the fem avoidable for the Helmholtz equation considering high wave numbers SIAM J. Numer. Anal.,34(6):2392-2423, December 1997.

[3] Zhongying Chen, Dongsheng Cheng, Wei Feng, and TINGTING Wu. An optimal 9-point finite difference scheme for the Helmholtz equation with PML. Int. J. Numer. Anal. Model, 10:389-410, 2013.

[4] Zhongying Chen, Tingting Wu, and Hongqi Yang. An optimal 25-point finite difference scheme for the helmholtz equation with PML. Journal of Computational and Applied Mathematics, 236(6):1240-1258, 2011.

[5] Björn Engquist and Andrew Majda. Absorbing boundary conditions for numerical simulation of waves. Proceedings of the National Academy of Sciences, 74(5):1765-1766, 1977.

[6] Gregory E. Fasshauer. Meshfree Approximation Methods with Matlab. World Scientific, 2007.

[7] J.C. Fabero, A. Bautista, and L. Casasus. An explicit finite differences scheme over hexagonal tessellation. Applied Mathematics Letters, 14(5):593-598, 2001.

[8] Bengt Fornberg and Natasha Flyer. A primer on radial basis functions with applications to the geosciences, volume 87. SIAM, 2015.

[9] Daniel T. Fernandes and Abimael F. D. Loula. Quasi-optimal finite difference method for Helmholtz problem on unstructured grids. International Journal for Numerical Methods in Engineering, 82(10):1244-1281,2010.

[10] Bengt Fornberg, Elisabeth Larsson, and Natasha Flyer. Stable computations with Gaussian radial basis functions. SIAM Journal on Scientific Computing, 33(2):869-892, 2011.

[11] Bengt Fornberg, Erik Lehto, and Collin Powell. Stable calculation of gaussian based RBF-FD stencils. Computers & Mathematics with Applications, 65(4):627-637, 2013.

[12] Gregory E. Fasshauer and Michael J. McCourt. Stable evaluation of Gaussian radial basis function interpolants. SIAM Journal on Scientific Computing, 34(2):A737-A762, 2012.

[13] Jun Fang, Jianliang Qian, Leonardo Zepeda-Nu~nez, and Hongkai Zhao. Learning dominant wave directions for plane wave methods for high-frequency Helmholtz equations. Research in the Mathematical Sciences, 4(1):9, May 2017.

[14] Taeyoung Ha and Imbunm Kim. Analysis of one dimensional Helmholtz equation with PML boundary. Journal of Computational and Applied Mathematics, 206(1):586-598, 2007.

[15] Y.C. Hon and R. Schaback. On unsymmetric collocation by radial basis functions. Applied Mathematics and Computation, 119(2):177- 186, 2001.

[16] Frank D Hastings, John B Schneider, and Shira L Broschat. Application of the perfectly matched layer (PML) absorbing boundary condition to elastic wave propagation. The Journal of the Acoustical Society of America, 100(5):3061-3069, 1996.

[17] Frank Ihlenburg and Ivo Babuska. Dispersion analysis and error estimation of Galerkin finite element methods for the Helmholtz equation. International journal for numerical methods in engineering, 38(22):3745-3774, 1995.

[18] Lise-Marie Imbert-Gerard. Interpolation properties of generalized plane waves. Numerische Mathematik, 131(4):683-711, Dec 2015.

[19] Edward J Kansa. Multiquadric a scattered data approximation scheme with applications to computational fluid-dynamicslii solutions to parabolic, hyperbolic and elliptic partial differential equations. Computers & mathematics with applications, 19(8-9):147-161, 1990.

[20] Seungil Kim and Joseph E. Pasciak. Analysis of a cartesian PML approximation to acoustic scattering problems in R2. Journal of Mathematical Analysis and Applications, 370(1):168-186, 2010.

[21] Seungil Kim and Joseph E. Pasciak. Analysis of the spectrum of a cartesian perfectly matched layer (PML) approximation to acoustic scattering problems. Journal of Mathematical Analysis and Applications, 361(2):420-430, 2010.

[22] Elisabeth Larsson, Erik Lehto, Alfa Heryudono, and Bengt Fornberg. Stable computation of differentiation matrices and scattered node stencils based on gaussian radial basis functions. SIAM Journal on Scientific Computing, 35(4):A2096-A2119, 2013.

[23] Leevan Ling, Roland Opfer, and Robert Schaback. Results on meshless collocation techniques. Engineering Analysis with Boundary Elements, 30(4):247-253, 2006.

[24] Leevan Ling and Robert Schaback. Stable and convergent unsymmetric meshless collocation methods. SIAM Journal on Numerical Analysis, 46(3):1097-1115, 2008.

[25] Pankaj Mishra, Sankar Nath, Gregory Fasshauer, and Mrinal Sen. Frequency- domain meshless solver for acoustic wave equation using a stable radial basis-finite difference (RBF-FD) algorithm with hybrid kernels, 4022-4027, 2017.

[26] Pankaj K. Mishra, Sankar K. Nath, Gregor Kosec, and Mrinal K. Sen. An improved radial basis-pseudospectral method with hybrid gaussian-cubic kernels. Engineering Analysis with Boundary Elements, 80(Supplement C):162-171, 2017.

[27] J. W. Nehrbass, J. O. Jevtic, and R. Lee. Reducing the phase error for finite-difference methods without increasing the order. IEEE Transactions on Antennas and Propagation, 46(8):1194-1201, Aug 1998.

[28] H. Power and V. Barraco. A comparison analysis between unsymmetric and symmetric radial basis function collocation methods for the numerical solution of partial differential equations. Computers & Mathematics with Applications, 43(3):551-583, 2002.

[29] Per-Olof Persson and Gilbert Strang. A simple mesh generator in Matlab. SIAM Review, 46(2):329-345, 2004.

[30] Robert Schaback. Multivariate interpolation and approximation by translates of a basis function. Series In Approximations and Decompositions, 6:491-514, 1995.

[31] J. Strikwerda. Finite Difference Schemes and Partial Differential Equations, Second Edition. Society for Industrial and Applied Mathematics, 2004.

[32] A. I. Tolstykh and D. A. Shirobokov. On using radial basis functions in a "finite-difference mode" with applications to elasticity problems. Computational Mechanics, 33(1):68-79, Dec 2003.

[33] Yi Tao and Mrinal K Sen. Frequency-domain Full Waveform Inversion with plane-wave data. Geophysics, 78(1):R13-R23, 2012.

[34] Holger Wendland. Scattered data approximation, volume 17. Cambridge university press, 2004.

[35] Holger Wendland. On the stability of meshless symmetric collocation for boundary value problems. BIT Numerical Mathematics, 47(2):455-468, Jun 2007.

[36] Grady B Wright and Bengt Fornberg. Scattered node compact finite difference-type formulas generated from radial basis functions. Journal of Computational Physics, 212(1):99-123, 2006.

[37] Man-Wah Wong. An Introduction to Pseudo-Differential Operators. World Scientific Publishing Company, 2 edition, August 1999.

[38] Churl-Hyun Jo, Changsoo Shin, and Jung Hee Suh. An optimal 9-point, finite-difference, frequency-space, 2D scalar wave extrapolator. Geophysics, 61(2):529-537,1996

PARQUE SOLAR CASTILLA

ENTREGARÁ ENERGÍA AL CAMPO CASTILLA BAJO UN ESQUEMA DE AUTOGENERACIÓN

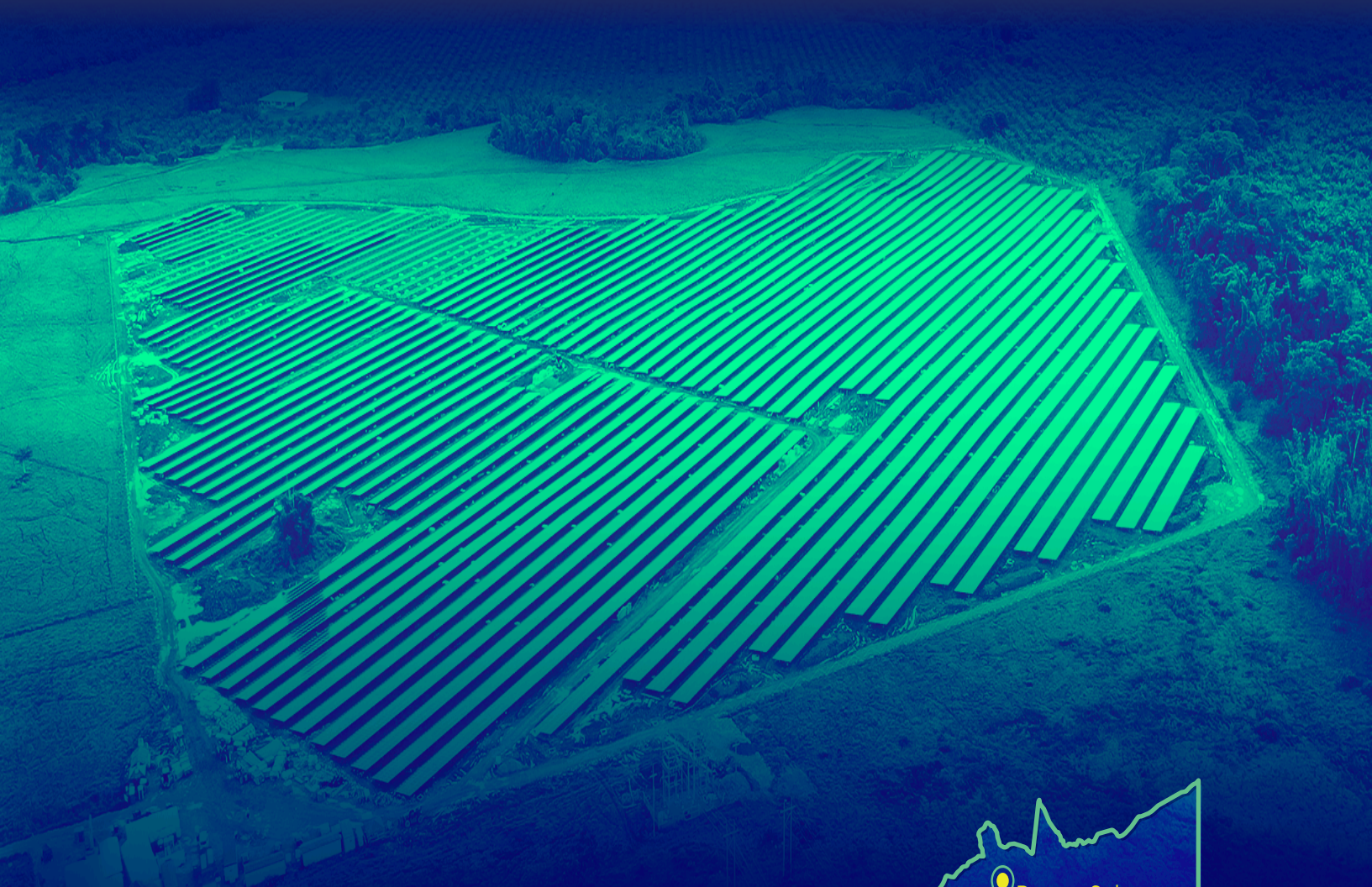

54.500 paneles solares
que transforman energía continua en energía alterna

18 hectáreas *equivalen a*
16 canchas de fútbol PROFESIONAL

Abastecerá de energía
CAMPO CASTILLA **15** años

Generó
388 empleos
29% fueron mujeres

Evitará la emisión de más de
154 MIL **TONELADAS DE CO_2**
equivalen a siembra de ***16.200 árboles***